ADDIS ABABA UNIVERSITY
ADDIS ABABA INSTITUTE OF THECHNOLOGY
SCHOOL OF MECHANICAL AND INDUSTRIAL ENGINEERING

Fracture Analysis of Shaft due to the Second Higher Critical Speed (Vibration) for AISI 1018 Steel Shaft

A Thesis Submitted to Addis Ababa University on

Partial Fulfillment of the Degree of Masters of Science in Mechanical Engineering (Mechanical Design)

By Semihar Ayalew

March, 2021

Advisor Dr. Samuel

Addis Ababa University
Addis Ababa, Ethiopia

Addis Ababa University
Addis Ababa Institute of Technology
School of Mechanical & Industrial Engineering

Fracture Analysis of Shaft due to the Second Higher Critical Speed (Vibration) for AISI 1018 Steel Shaft

Thesis Document

A thesis by

Name	Date	Signature

Approved by Board of Examiners

Advisor	Date	Signature

Name	Date	Signature

Internal Examiner

Name	Date	Signature

External Examiner

Name	Date	Signature

Faculty Dean

Name	Date	Signature

DECLARATION OF THE STATEMENT

I declare that no portion of the work referred in this thesis has been submitted in support of an application for another degree or qualification of this or any other university, and that all source of material is duly acknowledged.

A thesis by: **SEMIHAR AYALEW**

Thesis Title: **Fracture Analysis of Shaft due to the Second Higher Critical Speed (Vibration) for AISI 1018 Steel Shaft**

Department: _____

Signature: _____

Advisor: _____

Signature: _____

ACKNOWLEDGEMENT

I would like to take this opportunity with great pleasure to thank God and all individuals who really supported me in every steps of my education process. First I would like to thank almighty God for his guidance throughout my life. My sincerer gratitude goes to my dear family for everything they have done to me.

Then I will forward my acknowledgement to the School of Mechanical & Industrial Engineering and Addis Ababa Institute of Technology as well as Standard and Conformity Agency for allowing me to use whirling machine and SPERCTROMAX respectively. And my special thanks go to my advisor Dr. Samuel and Mechanical Design Chair Mr. Araya and my examiners Dr. Mulugeta and Dr. Haileleoul.

ABSTRACT

This paper was devoted to analyze fracture of shaft failure due to the second higher critical speed for AISI 1018 steel shaft. In this particular research, the influence of transverse cracks in a rotating shaft was analyzed by comparing with the un-cracked shaft which deflects at the second higher critical speed. The paper addressed the two distinct issues of the changes in critical speed and the influence of crack on dynamic response of shaft during operation. Moreover, the evolution of catastrophic failure of a cracked rotor near the second higher resonance frequency was investigated.

Numerical calculation was made to calculate the critical speed and other dynamic fracture parameters. ABAQUS was used to present the simulation result. The research utilized whirling machine for experimental investigation to find out the critical speed and the crack developed at the shaft. For homogeneity confirmation SPECTRO MAXX was employed.

The dynamic response obtained from simulation and experimental investigation was compared with those evaluated through numerical integration. It was observed that the critical speed of the cracked shaft decreases by 8.2% and 6.93%. Combined mode I & III of crack had been seen in the shaft.

Key words: Critical Speed, dynamic fracture, whirling of the shaft, AISI 1018 steel shaft, SPECTRRO max, ABAQUS

Table of Contents

LIST OF FIGURES

LIST OF TABLES

NOMECLATURES

SEM - Scanning electron microscope

1X - One times

2X - Two times

SAE - Society of Automotive Engineers

FFT - Fast Fourier transform

CCW – Counter clockwise

COD – Crack Opening Displacement

ω, V_c – Critical speed of shaft

l, X – Length of the shaft

E – Elastic modulus

I – Moment of inertia

J – Polar moment of inertia

g – Gravity

γ – Specific gravity

ω_i – Weight of the i^{th} location

y_i – The deflection at the i^{th} location

δ_i – Influence coefficient

$R_A \; and \; R_B$ - Load at point A and B

M – Moment of inertia

T - Torque

σ - Normal stress

τ - Shear stress

SFD - Shear force diagram

BED – Bending moment diagram

a – Notch depth

w – Notch width

K_I – Stress Intensity Factor for Mode I

K_{III} – Stress Intensity Factor for Mode II

σ_∞ – Externally imposed tensile stress far from the crack

D - Outer diameter of the shaft

d - Crack tip diameter

$\Gamma(v), G(l, v)$ – Energy Release rate

C_R - Rayleigh wave-speed

C_O – Speed of sound for one-dimensional wave propagation

V – Crack speed

w_f - Work of fracture

γs, - Surface energy.

σ_C – Cohesive stress

a_o – Initial crack length near plastic zone

DIN – Deutsche Industrie- Norm or German Industrial Standard

SERR – Strain Energy Release Rate

This page intentionally

left blank .

CHAPTER I

1.1. INTRODUCTION

In 1983, the National Bureau of Standards (now the National Institute for Science and Technology) and Battelle Memorial Institute (USA) estimated the costs for failure due to fracture to be $119 billion per year in 1982 dollars. The dollars are important, but the cost of many failures in human life and injury is infinitely more so [1].

Therefore, failure analysis has always been a source of interest for the technical and scientific community as a way through to the collection and analysis of data, to determine the cause and prevent mechanical failure, with the associated safety and economic benefits [2]. Mechanical failure can thus be defined as any change in size, shape, or materials properties of a structure, machine, or machine part that renders it incapable of satisfactorily performing the intended function [3].

There are numerous types of failure associated with shaft as well as other machine components and here the paper looked at the failure of rotor that was triggered due to higher critical speed. For several machines and devices, this kind of failure could bring a catastrophic failure in the shaft as well as in the machine as a whole.

1.1.1. SHAFT

A shaft is a rotating member usually of circular cross-section (solid or hollow), which is used to transmit power and rotational motion in machinery and mechanical equipment in various applications and controls the geometry of their motion [4]. An *axle* is a nonrotating member that carries no torque and is used to support rotating wheels, pulleys, and the like [5]. The automotive axle is not a true axle; the term is a carryover from the cab era when the wheels rotated on nonrotating members. A non-rotating axle can readily be designed and analyzed as a static beam, and will not warrant the special attention given in this research to the rotating shafts which are subject to dynamic loading.

Shafts do have many applications since antiquity. Even nowadays, shafts have a wide application from airplanes to nuclear plants and turbo generators as well to an enormous power plant to ordinary machines and devices (such as a watch).

Figure 1.1: Typical applications of rotors: (a) turbo-machinery (different stages); (b) ship propeller shaft; (c) backward curved fan; (d) gas recirculation fan [6]

Rotors are one of the most important components of rotating machines, which are widely used in many engineering fields. Because of the increasing need of energy, the plants installed by electricity supply utilities throughout the world are becoming larger and more highly stressed. Thus, the risk of turbo generator shaft cracking is increasing. Since the early 1970s when investigations on the vibrational behavior of cracked rotors began, numerous papers on this subject have been published, as a literature survey shows [7].

The shaft that is taken here is used for a turbo generator. Turbo-generator shafts are manufactured through the extrusion process. This results in the formation of weak planes in the direction of extrusion. They are exposed to both longitudinal and circumferential cracks when these shafts are subjected to higher critical speed. The dynamic response of these shafts could be severely affected by the presence of defects and crack opening.

Therefore, it is of vital significance to monitor and detect a crack, in order to reduce maintenance cost and avoid failure of a rotating machine. In addition, crack parameter identification can provide a foundation for life prediction of a cracked rotor [8].

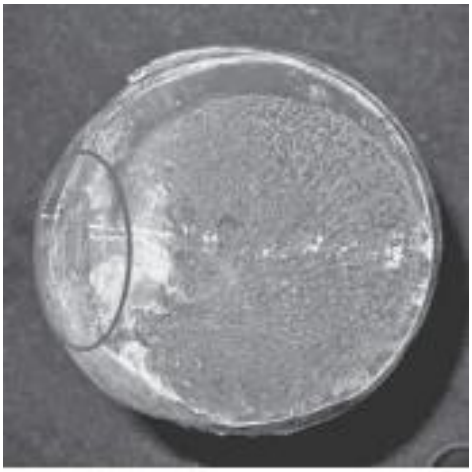

Figure 1.2: Fracture surface on broken part of shaft [9]

When a shaft is turning, eccentricity causes a centrifugal force deflection, which is resisted by the shaft's flexural rigidity *EI.* As long as deflections are small, no harm is done. At certain speeds, the shaft is unstable, with deflections increasing without upper bound [4].

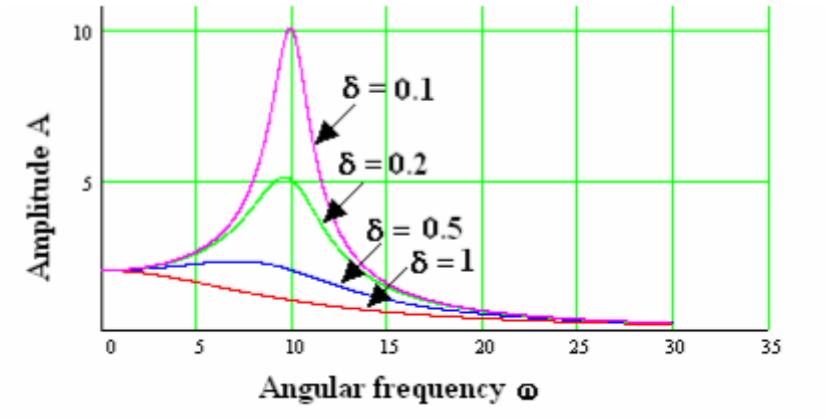

Figure 1.3: Amplitude versus Angular frequency[10]

Although rotors are carefully designed for fatigue loading and high level of safety by using high quality materials and precise manufacturing techniques, catastrophic failures of rotors as a result of cracks may still occur while operating at higher critical speed.

1.1.2. Critical Speeds of Shaft

In rotating machinery, there is a dynamic phenomenon called critical speed that is known to cause catastrophic driveline failures.

Alternative terminologies often found in the literature for this kind of phenomena are "critical angular velocity for synchronous precession," "critical speed of forward precession," and "critical whirling speed." Some authors simply refer to "natural frequencies," but risk the possibility of misunderstanding. For example, the natural frequencies of a nonrotating shaft will not always be close to the critical speeds.

The frequency, in which a system oscillates when not subjected to a repeated or continuous external load, is called its natural frequency [11]. Every single material possesses its own natural frequency. The excitation frequencies which cause other resonance phenomena in shafts are usually integral multiples of the operating speed. In general, the natural frequencies of a rotating shaft are a continuous function of the operating speed [12].

If something is hit at its natural frequency or a round multiple of it, then the amplitude of vibration increases in the transverse direction. In other way it means at the critical speed, the lateral bending frequency of the rotor shaft assembly is equal to the rotation frequency, resulting in very large radial displacement [13]. Therefore, the calculation of critical speed for any shaft is necessary to avoid the resonance of the shaft [14].

The magnitude of the deflection depends upon [15]:

- Stiffness of the shaft and its supports,
- The total mass of shaft and attached part,
- The unbalance of the mass concerning the axis of rotation, and
- The amount of damping in the system.

With the deflection, now considered as a function of speed, only the lowest (first) and occasionally the second are of interest to the designer, the others will usually be as high as to be well out of range of the operating speed.

At the first critical speed, the shaft will bend to the simplest shape possible. At the second critical speed it will bend to the second simplest shape possible etc. for example a shaft supported at its end and having a large (compared to a shaft) masses attached, will bend according to the configurations shown in figures 1 and 2 at the first and second critical speed respectively.

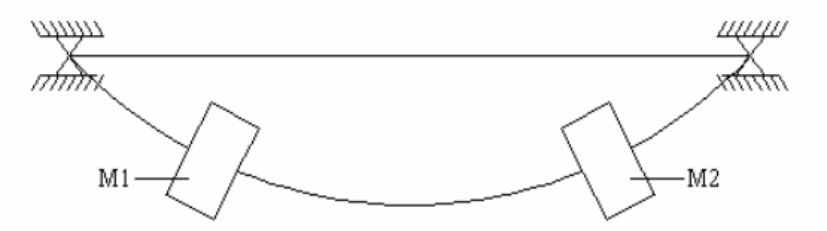

Figure 1.4: Loading configuration at the first critical speed [16]

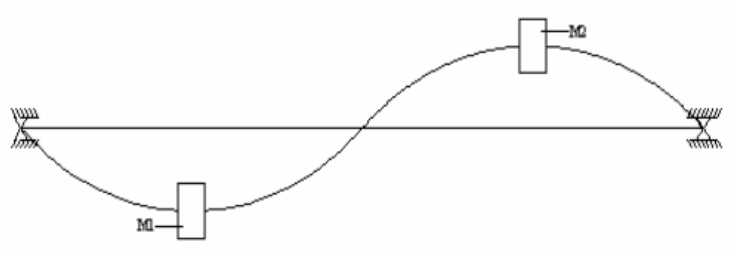

Figure 1.5: A variant of the Loading configuration at the first critical speed [16]

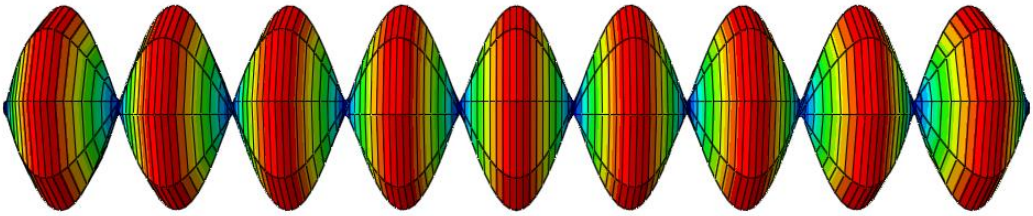

Figure 1.6: 29th mode of shaft without loading using ABAQUS

In engineering, many structures are prone to vibrate when resonated at or near the natural frequency. If the disturbance is close to the natural frequency, unpleasant & potentially dangerous failure will happen.

For δ is the damping ratio and ω_n the internal angular frequency. The following cases were described.

When $\delta > 1$ we have an over damped system.
When $\delta = 1$ we have a critically damped oscillation.
When $\delta < 1$ we have a damped oscillation that died away with time.
When $\delta = 0$ we have a system with no damping and a steady oscillation occurred.

It might be inferred from this pattern that if $\delta < 0$ we get an oscillation that grows with time. The diagram illustrates this pattern. As the energy is added to the amplitude grows and grows.

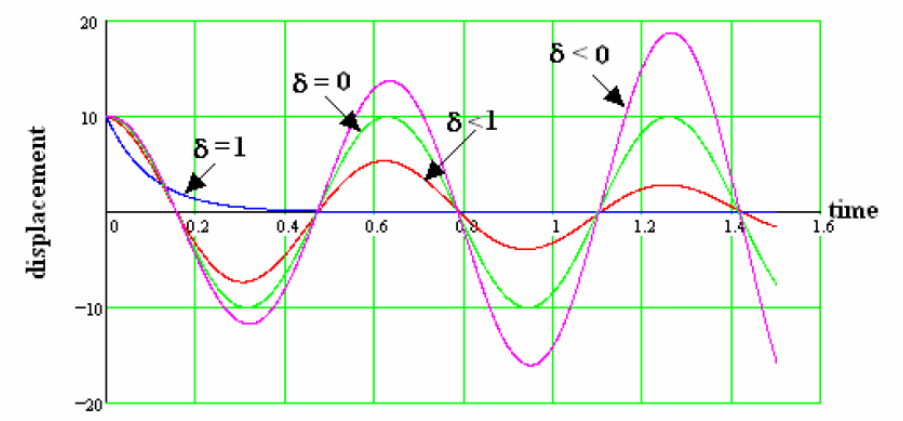

Figure 1.7: displacement with the damping ratio over time [10]

We may assume (and it is known from observations) that the mass is going to oscillate up and down with a sinusoidal oscillation of amplitude.

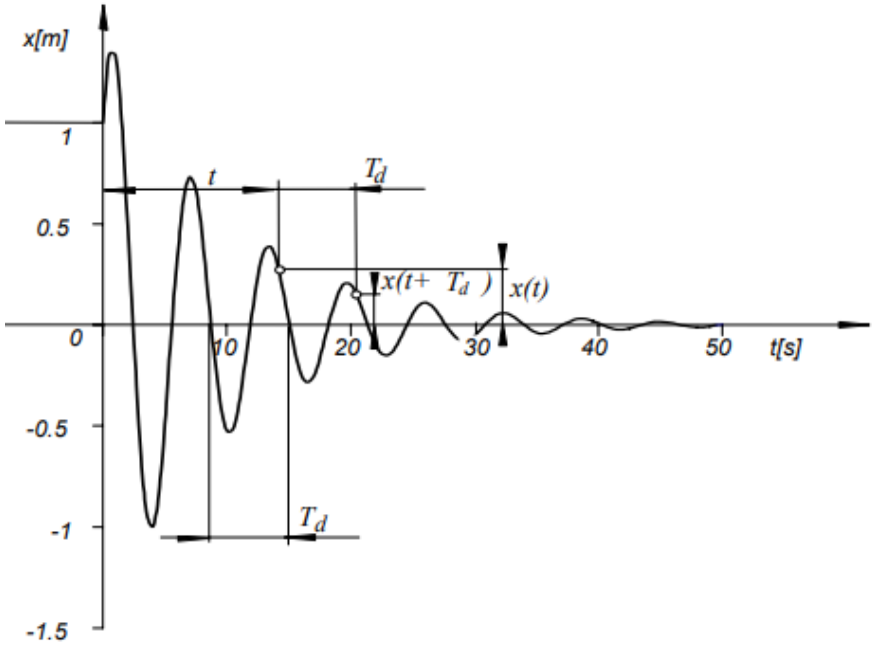

Figure 1.8: Natural logarithm of ratio of two displacements x(t) and x(t + Td) that are one period apart is called logarithmic decrement of damping and will be denoted by δ [13].

Concerning the instabilities of dynamic fractures, it has been observed that when the crack velocity *v* exceeds a critical speed *Vc*, the acoustic emission from the crack

increases [17; 18] the velocity oscillations are amplified and a pattern correlated with the velocity oscillations appears on the fracture surface [19].

The major remaining theoretical challenge is the determination of the dynamics of the crack [19], and the origin of the dynamic instability. There have been many suggestions to explain the motion of the crack tip. It has been argued [20] that conventional continuum theories are inadequate to describe the crack properties.

1.2. Problem statement

Shafts have been used for centuries to support wheel (as an axle or as a non-rotating member) and to transfer rotational speed. They have a very crucial role in different machines to transfer a rotational motion.

There seem to be many hindrances associated with shaft operation then. The most popular ones are fatigue and corrosion failure. However, failure associated with higher critical speed and the vibration is also the most catastrophic failure type in rotating shafts.

The presence of crack in a shaft has a significant effect on the critical speed of the shaft. Usually the critical speeds decrease due to crack. This sometimes leads to the operating speed to coincide with the natural frequency of the system if it is not detected early.

Rotors have a variable operating speed in which it makes them susceptible to excitation of the system. So, the downtime of the shaft can result from higher critical speed. Anyone can imagine the catastrophic failure that could bring total damage to the plant or the machine as a whole. This type of turbo generator failure incurs lot of money and a prolonged down time to the plant.

In this regard, the research is intended to find out and investigate the crack influence on the critical speed of the rotor and mode of shaft failure due to higher critical speed. In addition, the fracture behavior of the shaft will be studied to reckon the highest fracture energy that tends to bring a drastic failure to the system.

1.3. Objective

General objective

The main purpose of this thesis is to investigate the fracture of shaft failure due to the second higher critical speed for AISI 1018 steel shaft.

Specific objective

The particular objectives of this project are the following:

- ❖ Analytical analysis of critical speed and other dynamic fracture parameters.
- ❖ Analysis of the composition of material using SPECTROMAX.
- ❖ Modeling and simulation of the crack using ABAQUS
- ❖ Experiment to find out the whirling behavior of the machine around the second higher critical speed.

1.4. Methodology

For any investigation, the first and foremost step is to gather data. Data collection is the process of gathering information on targeted variables in a systematic way, which helps one to answer relevant questions and evaluate the outcomes. A detailed background investigation and literature review are important to identify probable factors for failure and fracture analysis.

The research is intended to follow a series of milestones to accomplish each task. Most (if not all) of these techniques are based on the theories of fracture mechanics and rotor dynamics. All in all, the methodology of the experiment includes three approaches:

1. Theoretical approach,
2. Simulation based approach and
3. Practical or Experimental approach.

The mathematical model of the experimental test bench is represented by a shaft with constant section, with horizontal axis, on which a disk is mounted.

There are various methods for estimating the critical speed, both analytically and experimentally. The analytical methods are briefly introduced, and then the experimental as well as simulation methods are more thoroughly discussed. Besides, the model is derived using ABAQUS as a commercial FEM program.

To capture the plastic behavior of the structure, a linear material model was used in the ABAQUS simulation.

Samples

Two different samples are taken from AISI 1018 steel shaft. A decrease in shaft discontinuities such as reduced sections, splines, riveted joints, bearings, and couplings will decrease the stress concentration area [5]. Therefore, the first sample was a smooth shaft with no discontinuity and no crack. The second sample has a crack that will initiate the actual crack for the shaft failure.

All in all, one sample for each case is considered to investigate the failure of turbo generator shaft at the second higher critical speed with standard sample size for whirling machine test.

Figure 1.9: methodology

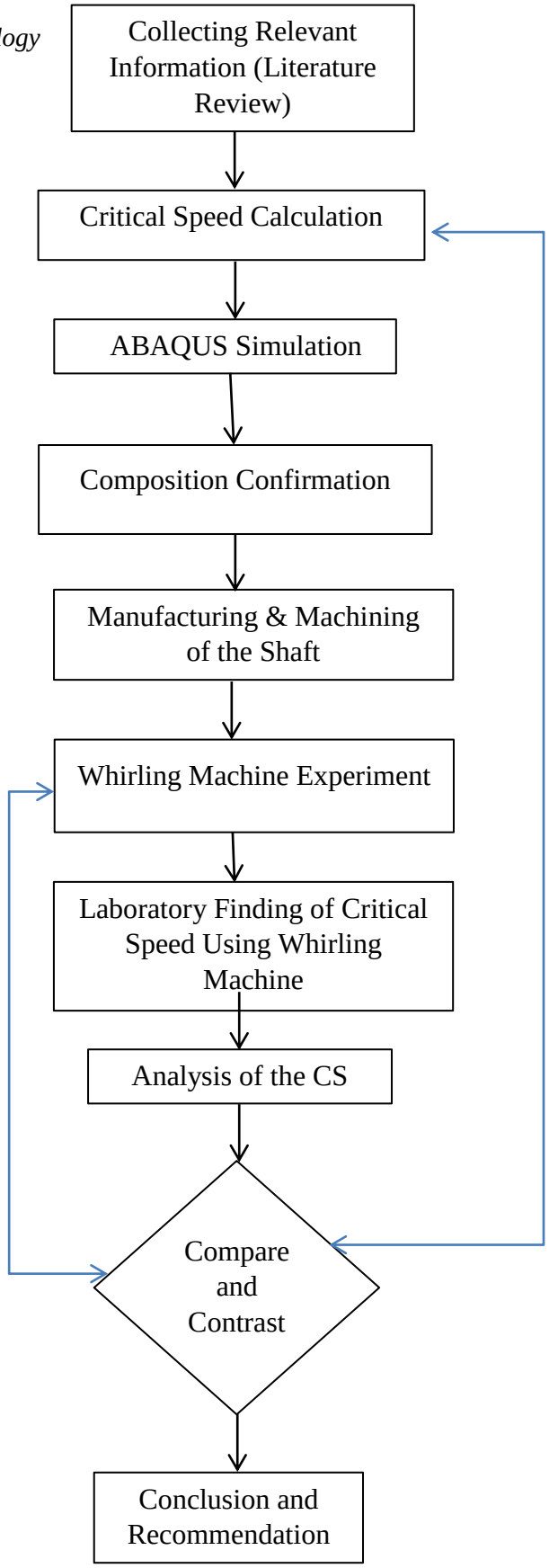

1.5. Significance of the research

Failure analysis is made to study the nature and the propagation of crack to prevent future damage to specific components. This helps us to develop a new material that can resist the former situation as well as prevent damage to the shaft during operation. Moreover, this study will aid in future machine design.

Generally speaking, this research will feed new information on the type of shaft failure encountered by high resonance. The SAE standard for the operation of the rotor must be revised in some way to incorporate crack during operation which degrade the critical speed.

1.6. Scope of the Research

Here the theoretical & practical analysis as well as the simulation will be executed. Then the results from all will be compared and contrasted to prove the consistency of each finding. The analysis is only made for AISI 1018.

1.7. Expected outcome

Here all the objectives are assumed to be attained. And the general outcomes are listed as follows:

1. The critical speed of the shaft
2. Stress intensity factor and energy release rate
3. Fracture analysis of shaft
4. Numerical simulation and result using ABAQUS
5. Experimental results

The analysis part is broad. It starts with the crack initiation and imparts the mode and the propagation of the crack in detail.

1.8. Organization of the Thesis

The general details of the thesis are described in this chapter. Chapter 2 presents a critical review of the literature on the types of shaft cracks, their causes, the characteristics of cracked shafts and the different literature that have been presented on the rotor failure due to critical speeds. The review establishes the need for this

research and the appropriateness of methods chosen. The configuration and preparation of the two different types of shaft specimens and different procedures are described in Chapter 3. Details of experimental study of the cracked and intact shafts are reported in Chapter 4. Analysis of the dynamic behavior of cracked and intact shafts is presented in Chapter 5. The summary and general conclusions along with future recommendations are presented in Chapter 6.

CHAPTER II

LITERATURE REVIEW

2.1. Failure Associated with Critical Speed

Rotating machinery such as compressors, turbines, pumps, jet engines, turbochargers, etc., are subject to vibrations. These vibrations are broadly classified as synchronous (due to unbalance) or nonsynchronous such as caused by self-excited rotor whirling. Generally, in rotor dynamics there are three major areas of concern which are rotor critical speeds, system stability, and unbalance response.

Many researchers have employed to figure out the actual cause of the failure of the shaft. A researcher investigated the dynamic response of a rotor model with a transverse crack, by obtaining the governing equations and solving them numerically [21]. Another researcher investigated the frequency response of the shaft model with different crack depths and locations and showed that the 1X and 2X harmonics were excited.

Grabowski used modal analysis to study the vibration behavior of a turbine rotor containing a transverse crack. He reported that the crack excites 1X and 2X vibrations, which are independent of the out-of-balance but depend on the crack location [22].

During the past several decades, a significant amount of research has been conducted in the area of crack detection in systems using only theoretical modeling method [3; 23] combined both theoretical and experimental methods [24] and only experimental method. The main idea of these approaches is that a change in a rotor system due to damage crack will manifest itself as changes in the rotor dynamic behavior. First of all, the presence of a transverse crack induces a slight decrease of the natural frequencies [25]. Secondly, resonances appear when the rotational speeds of the shaft reach 1/2 and 1/3 of the critical speeds of the rotor system. Therefore, with the increase of the crack depth, the 1/2 and 1/3 sub-critical resonant peaks increase [26]. Finally, some researchers [27] indicated that the shaft executes two and three loops per shaft revolution at the 1/2 and 1/3 sub-critical speeds, respectively.

A crack occurring in the rotating shaft of a turbo-generator will cause the system to vibrate abnormally, which may not be noticed during operation. Detection of a crack in its early stages may save the rotor from irreparable damage. By monitoring the type and severity of the crack, it is possible in some cases to extend the useful life of a cracked rotor without risking a catastrophic failure while arrangements are being made for a replacement. To implement such monitoring, a vibration of rotor systems with a crack has been studied extensively [28].

Figure 2.1: Fractured shafts [29]

As a result of continuing demand for increased performance, many modern turbo machines for petrochemical and natural gas service are now being designed for operation at shaft speeds approaching the second critical speed. In fact, machines have been purchased & delivered that operated so near a critical speed and difficulty was encountered to maintain the rotor balance required to ensure acceptable vibration levels [30].

Many researchers have focused on the shaft model and the dynamic response of a cracked rotor. If the bearings and housings were soft compared with the shaft, as in short shafts, then at the first two critical speeds, the shaft would bounce and pitch as a rigid beam [4]. The displacement may become so great that any number of failure modes are experienced; however, the classic critical speed failure mode is shaft buckling. Two researchers obtained some distinguishing features of a cracked rotor by examining the evolution of the first critical speed, associated amplitudes at the critical speed and half of the critical speed, and the resulting orbits during transient operation [31].

The avoidance of potentially dangerous vibrations through careful modeling of the shaft-bearing system should be undertaken early in the design process. The SAE design guideline suggests that the maximum operating speed should be less than 75-85% of the critical speed calculated by the elementary beam-theory method [32]. Sometimes there is sub-harmonic resonance occurs and causes the acceleration of degradation [33]. Although a shaft may be sufficiently strong to meet service life requirements, it may not be sufficiently stiff (or soft) to avoid rotor dynamics problems. Modern high speed rotating machinery can be designed to operate at speeds substantially greater than the fundamental critical frequency (so-called supercritical shafting), but proper attention to balancing and provisions for damping is usually required [34].

Figure 2.2: Critical speed failure of a driveshaft that resulted in buckling failure [34]

Most of the time, shaft failure is associated with stress concentration areas. The failures causes were more allied to welds, subsurface defects, and discontinuities. Because of the vibration issue of loosely fit shaft weld plugs were used which resulted in stress concentration [35]. As a matter of fact, many of the properties of materials are profoundly sensitive to deviations from crystalline perfection; the influence is not always adverse, and often specific characteristics are deliberately fashioned by the introduction of controlled amounts or numbers of particular defects [36]. And this defect can influence the creation of crack. Local yielding of notches, fillets, and other points of stress concentration is to be expected for shafts designed for short service lives (less than about 1000 cycles) [37].

The increased unbalance forces at the ends of the shafts sometimes cause the universal joints or other shaft connections to fail, and then parts go flying. These parts have a lot of energy and can-do a significant damage. Due to this machine

components are provided with the casing cover. And it is a well-known fact that the foundation of big plants is designed to accommodate such vibrations.

Rotating shafts are extensively implemented for power transmission in different industries. Most machinery may encounter torsional vibration in their rotary elements. Such vibrations could be caused by environmental shocks, random exciting torque, disturbance of electricity, or interaction of different parts of the system like shafts and bearings. However, the most common type of vibration which occurs in rotary systems is the torsional vibration of elements due to the resonance phenomenon. In such a case, vibration amplitudes may grow quickly to an unacceptable value, by approaching rotational speed to the natural frequencies of the system. The demands for higher operational speeds have been increased and resonance instability in such speeds can lead to drastic accidents [38].

Even some findings depict that with dry bearings it is apparent that the dry friction forces arising from the bearings can have an appreciable effect on the nature of the shaft vibrations [39]. When the rotor unbalances was small, *i.e.*, when the shaft was whirling with support at the inner edges of the bearings only, the shaft did not always have the same critical whirling speed. Further investigations of this phenomenon showed that when the temperature of the oil leaving the bearing increased, the critical whirling speed decreased [40]. It appeared, therefore, that the viscosity of the lubricating oil in the bearings had an effect on the whirling of the shaft, and tests were carried out to investigate this effect.

There appear to be three types of motion of the system: at speeds below this critical speed there is a rocking (jerking movement) of the shaft in the bottom of the bearings resulting in a predominantly lateral vibration of the rotor; as the shaft speed increases the rotor whirls in a normal manner; and as the shaft speed is decreased from a speed above the critical, the rotor vibrates predominantly in a vertical plane, due to bouncing of the shaft in the bearings. Rotor Dynamics to be ensured to avoid critical speeds in the operating range [41]. An appreciable increase in bearing clearance appears to result in the spreading of these phenomena over a larger frequency range. There is an identifiable natural frequency change that can be tracked with the seeded fault condition of the shaft [42].

Torsional vibration is similar to lateral vibration after shaft twist has been substituted for shaft bending. Torsional excitations and stress and motion mechanisms, including critical speeds, simple and complex harmonic motions, transient and self-excited motions are described [43]. In extremely critical situations failure can occur during a single start-up. It has analyzed such a failure and documented the corrective action taken [44].

Delimitation

The above pieces of literature only show the evidence of a crack in the shaft due to higher critical speed. It is therefore, there must be research that clearly shows the crack mode on this type of shaft failure. Again, the crack propagation needs to be studied to see what happens when the shaft is subjected to higher critical speed. Generally, the fracture analysis of shaft failure due to the critical speed has got a little attention in the above review.

2.2. Dynamic Fracture

Dynamic fracture is a branch of the engineering science of fracture mechanics concerned with fracture phenomena on a time scale for which inertial resistance of the material to motion is significant. The deformable body typically contains a dominant crack or other stress concentrating defect, and the phenomena of primary interest are those associated with conditions for the onset of extension of a crack or its arrest. Material inertia can have a significant effect in a variety of ways. Load transfer from the rapidly loaded boundary of a body to the region of a crack edge can occur employing stress waves. Likewise, a rapidly running crack emits stress waves which can be geometrically reflected or scattered back to the region of the crack [45].

Researchers have considered the Timoshenko shaft with a transverse crack which opens and closes during motion. It has been represented by generalized forces and moments [46].

Different scholars [47; 48] have suggested that it is easier to detect cracks during start-up or run-down process than at steady speed. Researchers [49; 50] presented an analysis of the on-line measurement of cracked turbo-generator rotors during passage through the critical speed. Investigations on the response of a cracked rotor passing through critical speed [51] and also through subcritical resonances [52] have been

carried out. Two investigators [28] compared the response of a cracked rotor with an asymmetric rotor. When the driving force for crack extension exceeds the material resistance, the structure is unstable, and rapid crack propagation occurs [53].

2.3. Crack

A simple crack is defined as a single crack that propagates along a single (straight) fracture plane. It is, basically, a crack that does not undergo any path instabilities [54].

Cracks that open on the surface are known as surface cracks; cracks which are not visible on the surface are known as subsurface cracks [55].

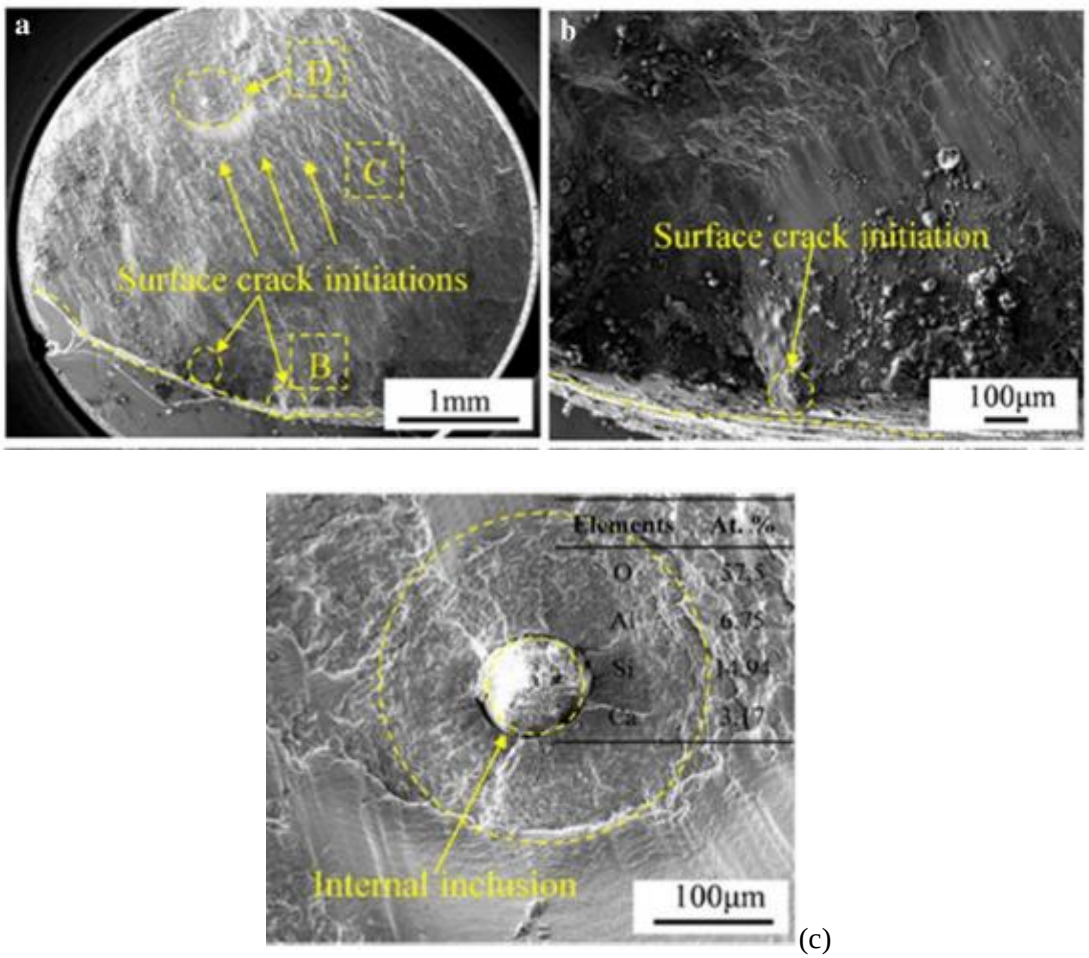

Figure 2.3: Fracture morphology of the specimen failed at WM at room temperature: the overall morphology of fracture surface, b magnified micrograph of one surface crack initiation, c internal inclusion in the final fracture zone [56]

Slip, dislocation movements, or fracture release energy manifested as a propagating stress wave. In rotating, shafts, the high stress levels are found in highly regions just near the crack propagation [57].

The classical theory of fracture mechanics states that a crack propagating in an unbounded body should smoothly accelerate until it reaches the Rayleigh wave speed [58]. At higher velocities V_B *(>* V_C*)* a macroscopic branching instability occurs; the crack tip splits or deviates from its original direction [45].

2.4. DUCTILE FRACTURE

The material eventually reaches an instability point, where strain hardening cannot keep pace with the loss in the cross-sectional area, and a necked region forms beyond the maximum load. In very high purity materials, the tensile specimen may neck down to a sharp point, resulting in extremely large local plastic strains and nearly 100% reduction in area. Materials that contain impurities, however, fail at much lower strains. Micro-voids nucleate at inclusions and second-phase particles; the voids grow together to form a macroscopic flaw, which leads to fracture [59].

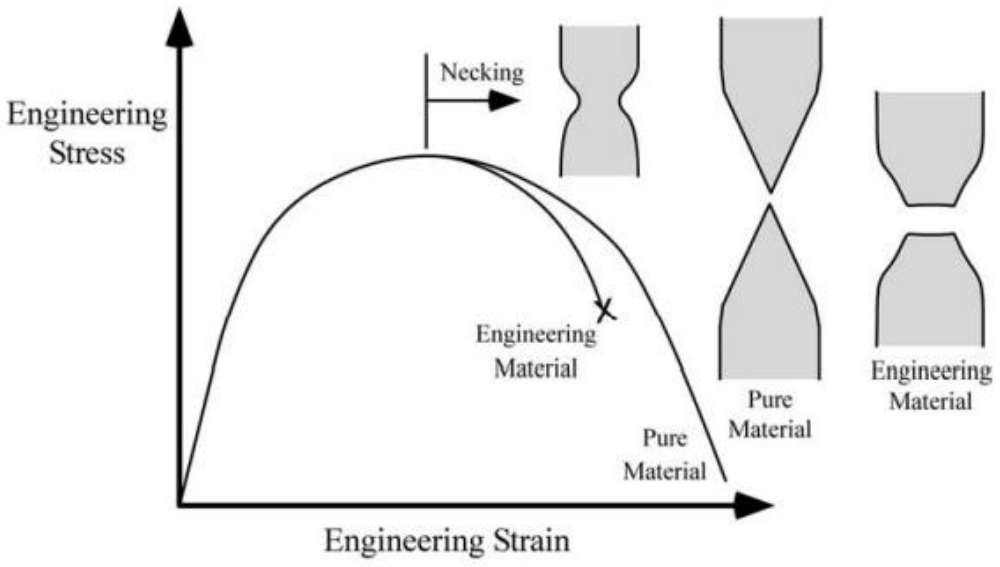

Figure 2.4: Uniaxial tensile deformation of ductile materials [59]

For the wide range of yield fracture problems and all yield fracture problems that have a large plastic zone at the end of the crack, linear elastic fracture theory is no longer applicable, the elastic-plastic fracture theory must be used to analyze. At present, there are many kinds of methods of searching the elastic-plastic fracture, but the COD method and j-integral method are the most common.

In tougher materials bond rupture plays a relatively small role in resisting crack growth, which by far the largest part of the fracture energy being associated with

plastic flow near the crack tip. A "plastic zone" is present near the crack tip within which the stresses as predicted by below would be above the material's yield stress σ_y [1].

$$\sigma_x = \frac{K_I}{\sqrt{2\pi r}}\cos\frac{\theta}{2}\left(1 - \sin\frac{\theta}{2}\sin\frac{3\theta}{2}\right) + \ldots$$

$$\sigma_y = \frac{K_I}{\sqrt{2\pi r}}\cos\frac{\theta}{2}\left(1 + \sin\frac{\theta}{2}\sin\frac{3\theta}{2}\right) + \ldots$$

$$\tau_{xy} = \frac{K_I}{\sqrt{2\pi r}}\cos\frac{\theta}{2}\left(\cos\frac{3\theta}{2}\sin\frac{\theta}{2}\right) + \ldots$$

2.5. Mode of the crack opening

Crack initiation

Tiny discontinuities are initiated in the un-cracked parent material during this stage. These cracks may be caused by mechanical stress raisers, such as sharp keyways, abrupt cross-sectional changes, heavy shrink fits, dents, and grooves, or factors such as fretting and/or metallurgical factors such as forging flaws, inclusions, porosity, and voids.

Crack propagation

During this stage, the discontinuity grows in size as a result of the cyclic stresses induced in the component. Certain conditions can accelerate the crack growth rate. Failure occurs when the material that has not been affected by the crack cannot withstand the applied stress. This stage happens very quickly.

2.6. Types of Cracks in Shafts

The geometry of cracks has an impact on the characteristics and dynamics of the cracked rotor. Therefore, cracks are categorized into three groups as follows.

Transverse Cracks

These kinds of cracks are the most serious and most common defects in rotating systems. They are perpendicular to the axis of a shaft as shown in the figure below.

They reduce the cross-sectional area of the shaft and produce serious damages to the shaft.

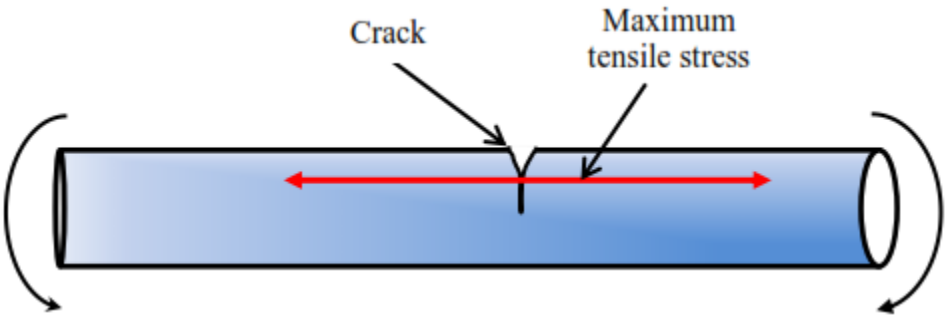

(*a*)

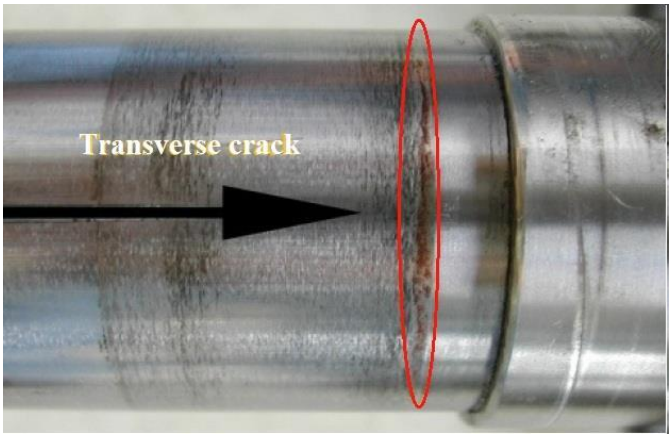

(b)

Figure 2.5: (a) and (b) transverse crack [6]

Longitudinal Cracks

This type of cracks is relatively uncommon and less serious, and it is parallel to the axis of the shaft as shown in figure.

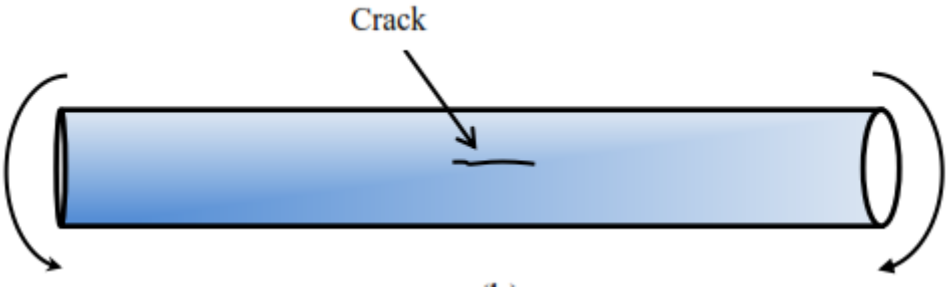

Figure 2.6: longitudinal crack [6]

Slant Cracks

This kind of cracks appears at an angle to the axis of the shaft. They occur less frequently compared to transverse cracks. Another nomenclature frequently

mentioned in the literature is “breathing crack”, in which the generated stresses around the cracked surface during rotation of the shaft depending on the circumferential location of the crack. The crack is open when the surface of the shaft is under tensile stresses and closed when the surface stresses reverse to compressive stresses and so on.

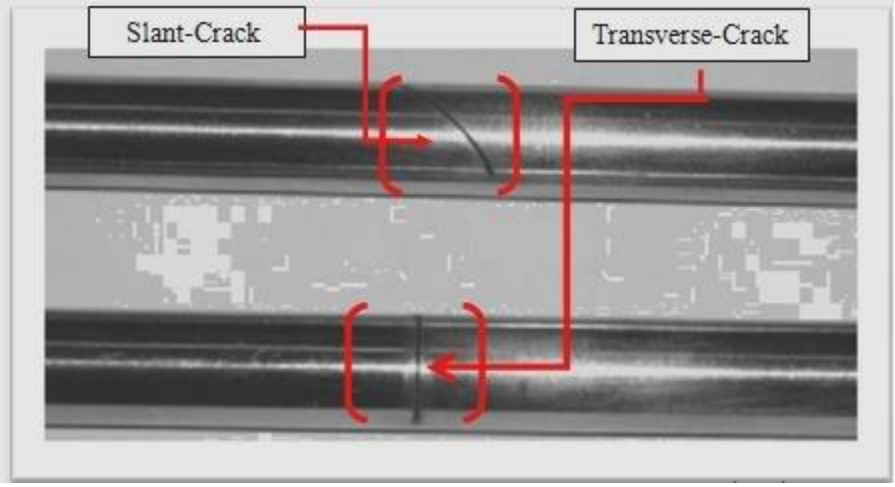

(a)

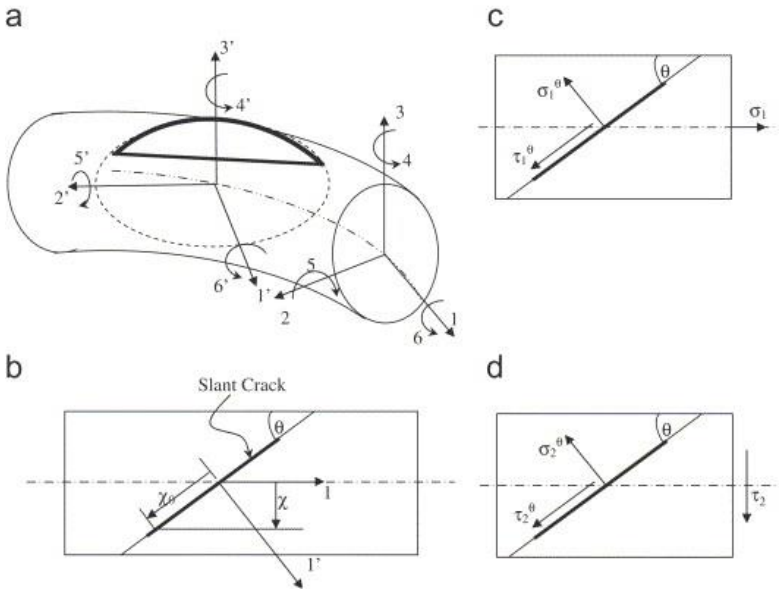

(b)

Figure 2.7: (a) slant and transverse crack in shaft [60]*(b) slant crack* [61]

2.7. The stress intensity approach

The stress intensity factors depend on the loading configuration and geometry of a given fracture problem. Once they are known, the energy release rate G can be readily calculated. The equation of motion for a straight crack is then given by Γ (v) = G.

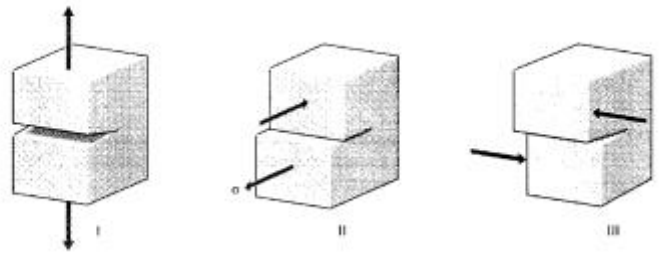

Figure 2.8: Fracture modes [62]

While the energy-balance approach provides a great deal of insight to the fracture process, an alternative method that examines the stress state near the tip of a sharp crack directly has proven more useful in engineering practice. The literature treats three types of cracks, termed mode I, II, and III as illustrated in the figure above. Mode I is a normal-opening mode and is the one the research should emphasize here together with Mode III, while modes II and III are shear sliding modes. The crack that is perpendicular to the direction of pull and through the thickness on the tensile plate belongs to mode I type fracture.

Mode II-type fracture belongs to the sliding mode fracture. The crack caused by the crack along the tangent direction belongs to II-type fracture. In addition, the rupture which the circumferential crack the cliff of the pipe on the torsional thin-walled circular tube forms under the effect of torque also belongs to II-type fracture.

Mode III-type fracture belongs to tear-shaped fracture. The crack which annular groove cutting or surface circumferential crack on circular shaft or the circular sample forms when the torsional effect of the circular shaft belongs to III-type fracture

2.8. ABAQUS

In order to effectively study strong discontinuity problems such as crack, ABAQUS provides two methods to simulate the crack problem. One is based on the conventional finite element method (CFEM) on the research of the crack problem;

this method requires the user to establish the model grid that is consistent with the actual situation of crack. Another method is based on extended finite element method (XFEM) for crack problem research; there is no need for the user to establish the model grid that is consistent with the actual situation of crack.

ABAQUS is a standalone FE-software which includes an explicit solver which is suitable for dynamic simulations. In addition, the explicit approach is also better suited when simulating high speed dynamic events, complex contact problems and problems with difficult material behaviors', such as crack propagation and degradation [63].

THE EXTENDED FINITE ELEMENT METHOD (XFEM)

The function of the newly launched in ABAQUS 6.9 is the extended finite element method (XFEM). It uses the extended finite element method (XFEM). Division of the grid has nothing to do with internal structure geometrical or physical interface, so in the crack tip mesh of high stress and deformation, high precision is no longer a problem, and at the simulation of crack initiation we no longer have to divide the grid subdivision again.

Crack domain

To define the crack domain, you can select one or more cells from three-dimensional parts or one or more faces from two-dimensional planar parts. If you are defining the crack domain on an orphan mesh or a part containing both orphan and native mesh elements, you can select elements. The crack domain includes regions that contain any existing cracks and regions in which a crack might be initiated and into which a crack might propagate.

Crack growth

You can allow the crack to propagate along an arbitrary, solution-dependent path, or you can specify that the crack is stationary.

Initial crack location

To define the initial crack location, you can select faces from a three-dimensional solid or edges from a two-dimensional planar model. The initial crack location must be contained within the crack domain. A selected face can be a face of the solid, a face created by a partition, or a planar part instance. Similarly, a selected

edge can be an edge of the solid, an edge created by a partition, or a wire part instance; you should not select a seam crack. You should not mesh the faces or edges that you selected to define the initial crack location. Figure shows examples of the crack domain and the crack location for two- and three-dimensional geometry and orphan meshes.

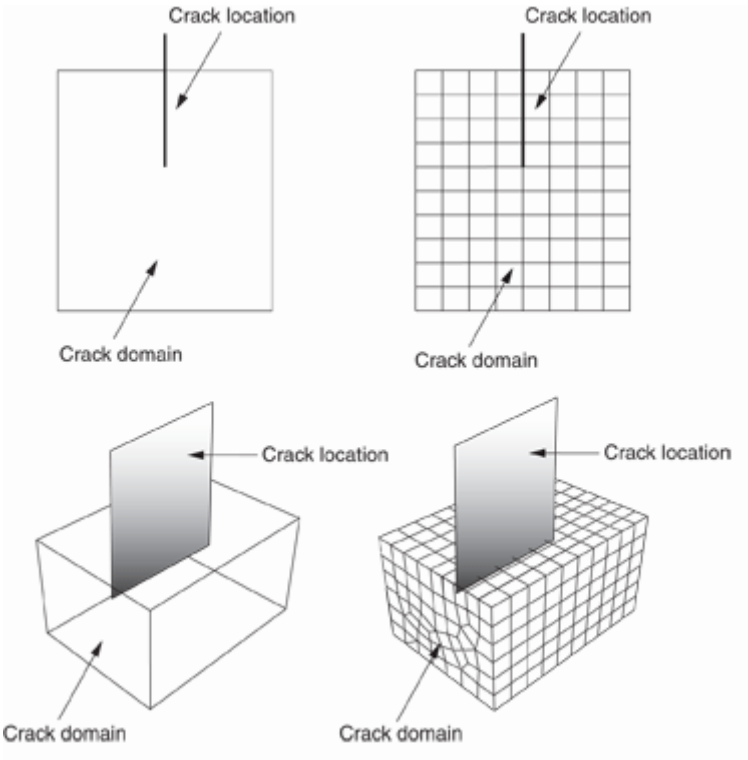

Figure 2.9: Defining a crack for XFEM.

Alternatively, you can choose not to define the initial crack location. Regardless of whether you define the initial crack location, ABAQUS initiates the creation of cracks during the simulation by searching for regions that are experiencing principal stresses and/or strains greater than the maximum damage values specified by the traction-separation laws.

CONTOUR INTEGRAL

If your part is three-dimensional, you must define the crack line by selecting edges or element edges that form a continuous line. The crack line is a series of connected edges along the crack front where you define the crack extension direction. In some cases the desired edges will not exist, and you must create them by partitioning the crack front. If you selected edges or element edges to define the crack front, the same edges define the crack line. Selected edges (from an ABAQUS/CAE native part or

from an orphan mesh) must be connected, must connect one side of the crack front to the other, and must be included in the crack front.

Figure 2.10: crack selection for contour integral

After you have defined the crack front along with the crack tip or crack line, ABAQUS/CAE prompts you to specify the crack extension direction at the crack tip or along the crack line. You can specify the normal to the crack plane, or you can specify the crack extension direction, , directly.

Normal to crack plane

If you select Normal to crack plane, you can define the normal by selecting points from the model that represent the start and the end of the normal to the crack plane. The crack plane contains the vector that ABAQUS needs to compute the contour integral. In many cases the crack plane represents the plane of symmetry of the crack.

You should define the normal to the crack plane only if the direction is the same at all points along the crack line. If the direction of the normal to the crack plane varies along the crack line, you cannot select a single normal that defines the crack extension direction at all points along the crack line.

q Vectors

If you select q vectors, you can define the crack extension direction, , directly by selecting points from the model that represent the start and end of the vector. If you are working with an orphan mesh part, you must select nodes that represent the start and the end of the vector. Alternatively, you can enter the coordinates of the points in the prompt area.

2.9. WHIRLING MACHINE

Whirling of shaft apparatus shows how shafts vibrate transversely and 'whirl' at a certain rotational frequency.

This helps engineers understand possible problems with long shafts. The main part is a solid alloy frame that holds a variable speed motor which turns the horizontal test shaft. Two bearings hold the shaft, one bearing at the 'driven end' and the other bearing at the 'other end' of the shaft. The motor end bearing slides in its housing to allow the shaft length to change as it 'whirls'. Similar to a beam on two simple edge supports, both bearings allow free angular shaft movement (free ends condition).

Two movable nylon bushes help to prevent the shaft whirling amplitude from excessive vibration. A movable cord plate allows the experimenter to control the shaft in some experiments, to help reach the second mode whirl speed. A sensor at the driven end measures the shaft speed and sends its signal to the Control and Instrumentation Unit display. A removable safety guard with a magnetic interlock surrounds the shaft and only allows the motor to work when fitted [64].

The separate Control and Instrumentation Unit contains the drive for the variable speed motor and a display to show the shaft speed. It also includes a trigger output for the optional stroboscope.

Figure 2.11: A whirling machine [65]

Whirling Machine and its specification

Dimensions

$L \times W \times h = 1150 \times 375 \times 355$ mm^3

Weight: 45 kg

Power supply: 230V 50Hz

Motor

Speed range 300 ... 3000 rpm

Output: 0.37 KW

Speed adjustment: two 10-speed switch-over potentiometers

Speed display: digital, 8-position, LCD

Rotor

Shaft

Material: steel, density: 7850 Kg/m3

Modules of elasticity 210000 N/mm^2

Diameter×Length 6×500 mm^2

Mass discs

Number: 2

Material: steel, density: 7850 Kg/m3

Diameter: 80 mm

Mass: 1.0 Kg

Minimal distance between discs: 50 mm

Bearing

Type: self-aligning bearing

No. of bearings: 2

Distance between bearings (Adjustable): 300…470 mm

Safety bearings (permanently mounted at mass disc)

Bearing gap: ±3 mm

2.10. SPECTRO Max

The SPECTRO MAXx is the most successful product in the history of SPECTRO and simultaneously probably the most successful metal analyser in its class on the market. In its fifth generation, the new SPECTRO MAXx once again offers improved performance and unconditionally efficient routine operation with minimal operating costs.

The SPECTRO MAXx is available as a bench top or floor unit in three different versions that vary in the available wavelength ranges and thus in the analytical capacities. All of the important elements required in the metal industry can be determined with this analyser, including traces of carbon, phosphorous, sulphur, and

nitrogen. Pre-defined calibration modules are available for the relevant bases, such as Fe, Al, Cu, Ni, Co, Ti, Mg, Zn, Sn, and Pb. These encompass the complete palette of relevant elements and can be adjusted to fit individual requirements [66].

Devised for the trouble-free execution of even the highest sample volumes, the SPECTRO MAX offers high reliability with minimal maintenance requirements in addition to simple operation and outstanding analytical performance.

A computer is used to display the result. Computer port (double-shielded 8-pin, for use with an external computer): plug one end of an 8-pin DIN serial cable into this port; the other end attaches to the serial (modem) port of the computer.

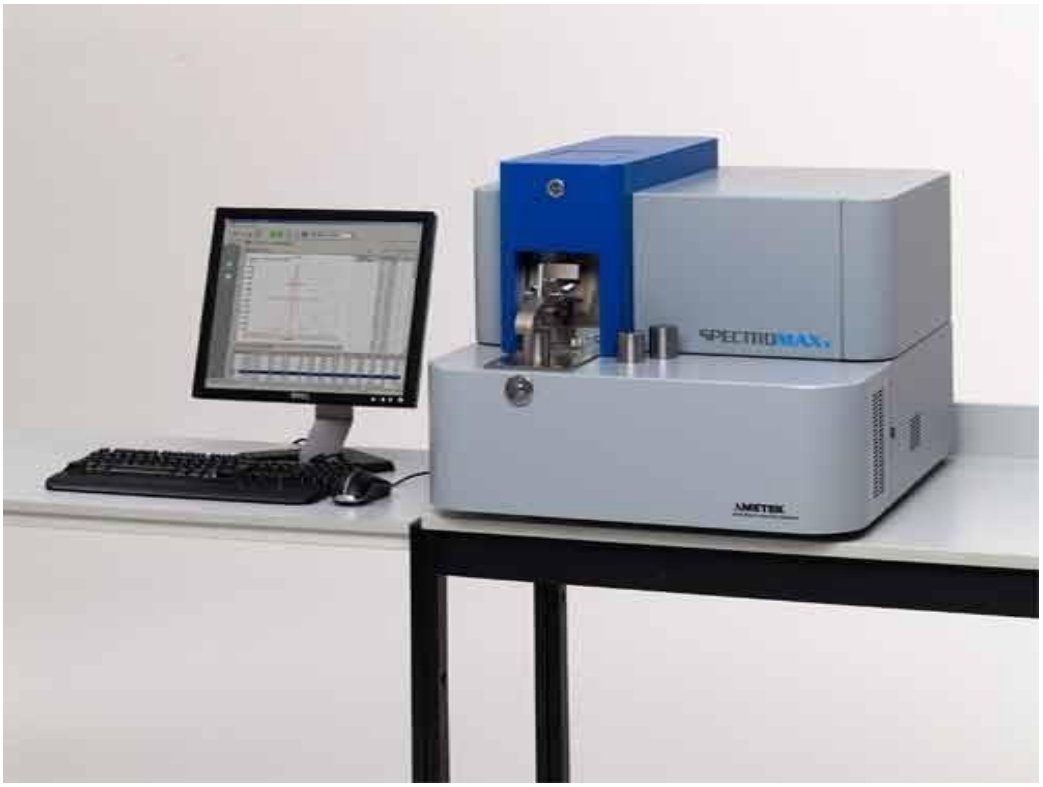

Figure 2.12: SPECTRO-max

CHAPTER III

PROCEDURES AND SETUPS

3.1. SPECTROMAX lab setup

Spectra-Max micro-plate spectrophotometers provide rapid and sensitive measurements of a variety of analysts across a wide range of concentrations. They measure the optical density (OD) of samples at selected wavelengths in a number of reading modes.

First a 6mm sample was prepared and clipped on the analyzer surface. Then a series of blue spark was emitted along the specimen. Results of the composition were displayed in the computer. And the test was repeated at least twice to check the validity of the percentage of the resulted chemical elements.

3.2. ABAQUS Simulation

Procedure

1) Pre-Processing

- Geometry Modeling
- Material and Contact Definition
- various Load
- various boundary condition
- Meshing

2) Solution &

3) Post-Processing

- Deformation (Dynamic)
- Stresses (Dynamic)

Geometry Modeling

The shaft is Ø6x480mm.

Figure 3.1: shaft profile

Material Properties

	Young's Modulus	Poisson's Ratio
1	210000	0.3

Load

The two masses are coupled with the shaft. And the two ends are constrained.

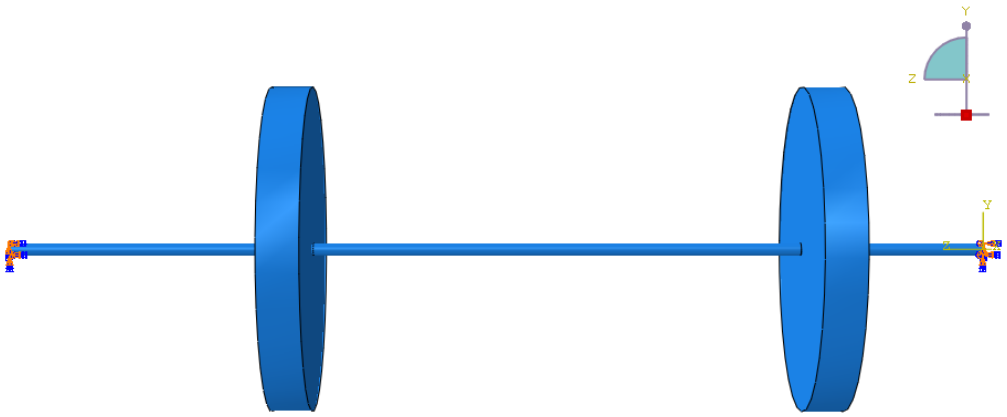

Figure 3.2: load with the boundary condition

The global mesh size was put to be 2 mm with mesh refinements of 0.8 mm on the discs and the shaft. This model was executed using ABAQUS dynamic explicit software. The mesh can be seen in figure below.

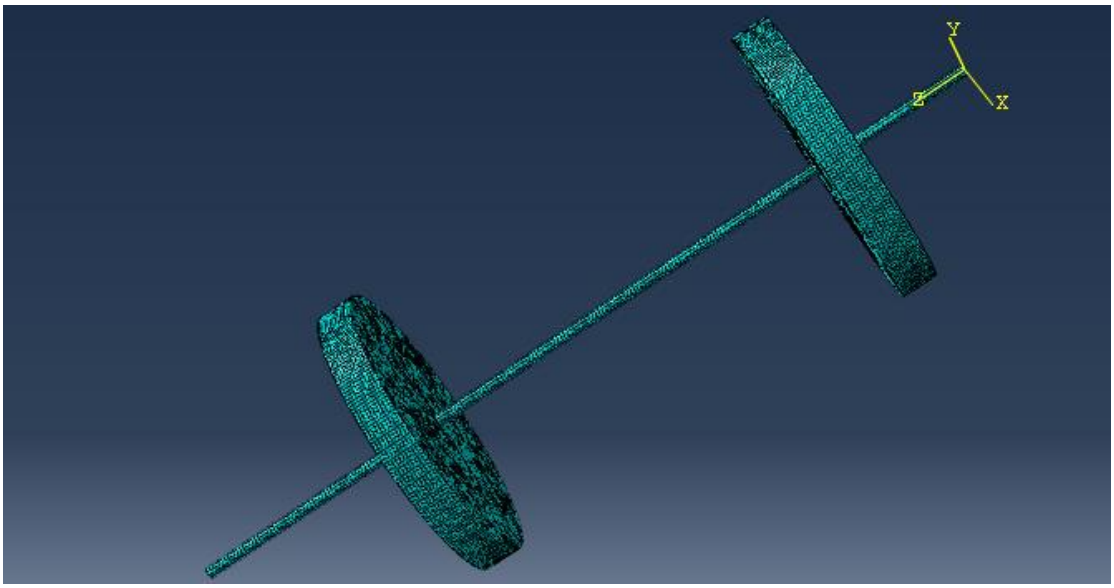

Figure 3.3: meshed un-cracked shaft

MODELING THE SHAFT FOR TORSION AND THE TWO CONCETRATED LOAD

The torque was applied to see the twisting effect on the shaft. One end of the shaft was constrained and the other end did allow a rotating load.

	Young's Modulus	Poisson's Ratio
1	210000	0.3

	Max Principal Stress
1	76000000

Damage Evolution

Type: Energy

Softening: Linear

Degradation: Maximum

Mixed mode behavior: Power Law

Mode mix ratio: Energy

☑ Power 0.37

☐ Use temperature-dependent data

Number of field variables: 0

Data

	Normal Mode Fracture Energy	Shear Mode Fracture Energy First Direction	Shear Mode Fracture Energy Second Direction
1	107000	107000	107000

Load

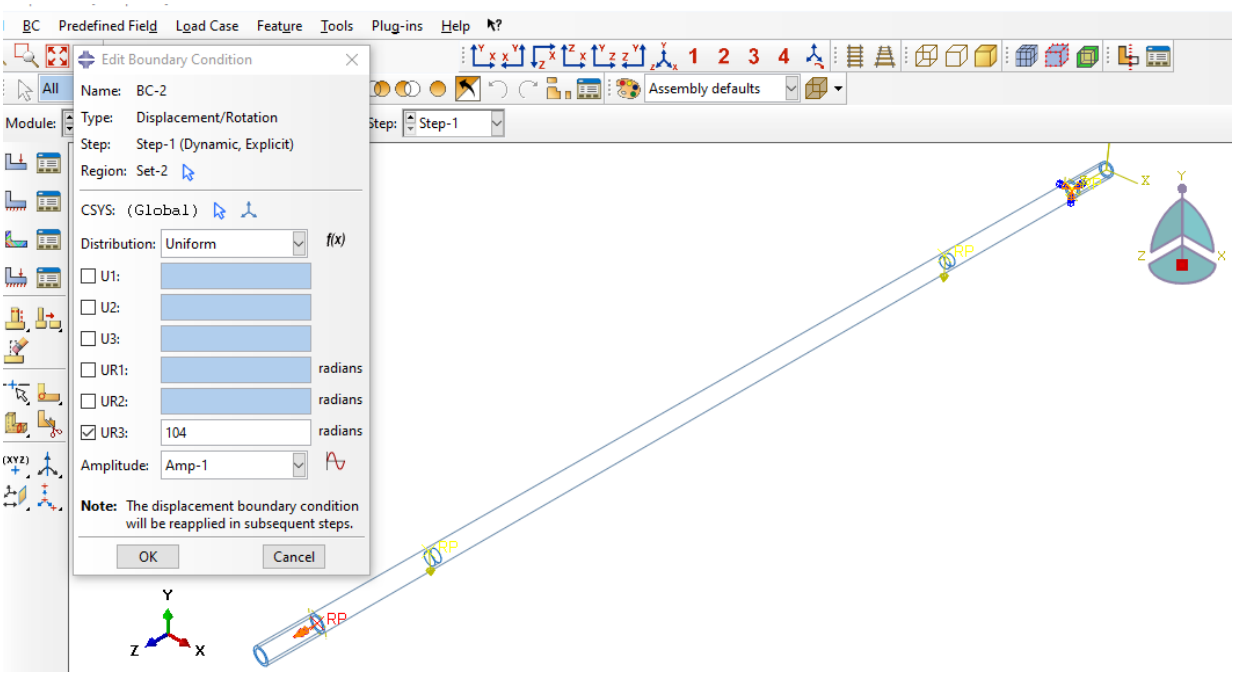

Figure 3.4: Loading Condition for torsion & bending with one end constrained

Figure 3.5: meshed shaft for Torsion and bending

Modeling the cracked Shaft

The global mesh size was put to be 3 mm with mesh refinements of 0.1 mm on the shaft. This model was executed using ABAQUS XFEM. The mesh can be seen in figure below.

Material properties

Data

	Young's Modulus	Poisson's Ratio
1	210000	0.3

Data

	Mass Density
1	7.8E-009

Data

	Yield Stress	Plastic Strain
1	220	0
2	324	0.15

MIXED MODE MODELING (MIXED LOADING) with initial crack

The crack was introduced using XFEM and the equivalent torque load and the bending load was applied on the shaft. The equivalent torque load was found by dividing the power with the angular speed which was found to be 3.53N.m.

Interaction

The crack was introduced using XFEM and allowed to propagate.

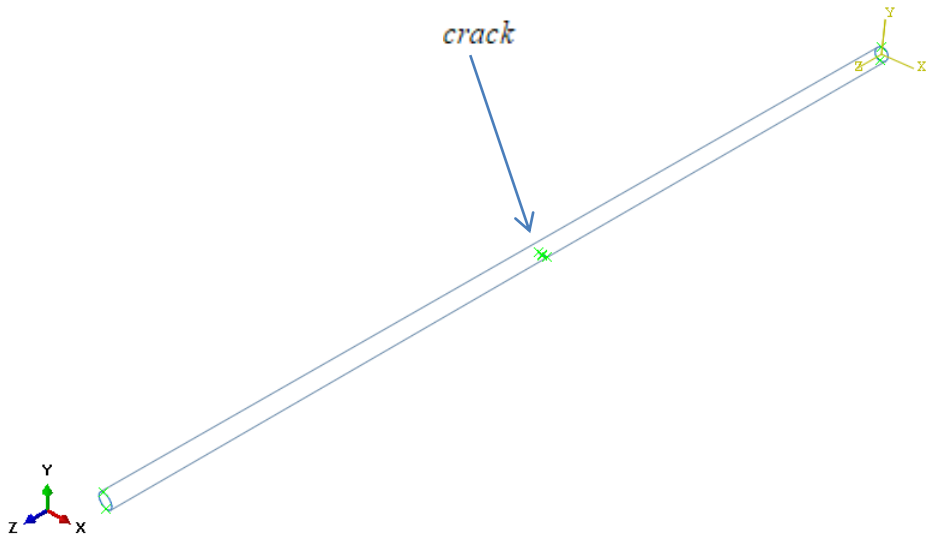

Figure 3.6: creating crack using XFEM for 1.8mm crack depth

Load

The load considered the maximum deflection resulted from torsional and bending analysis which is found in the appendix.

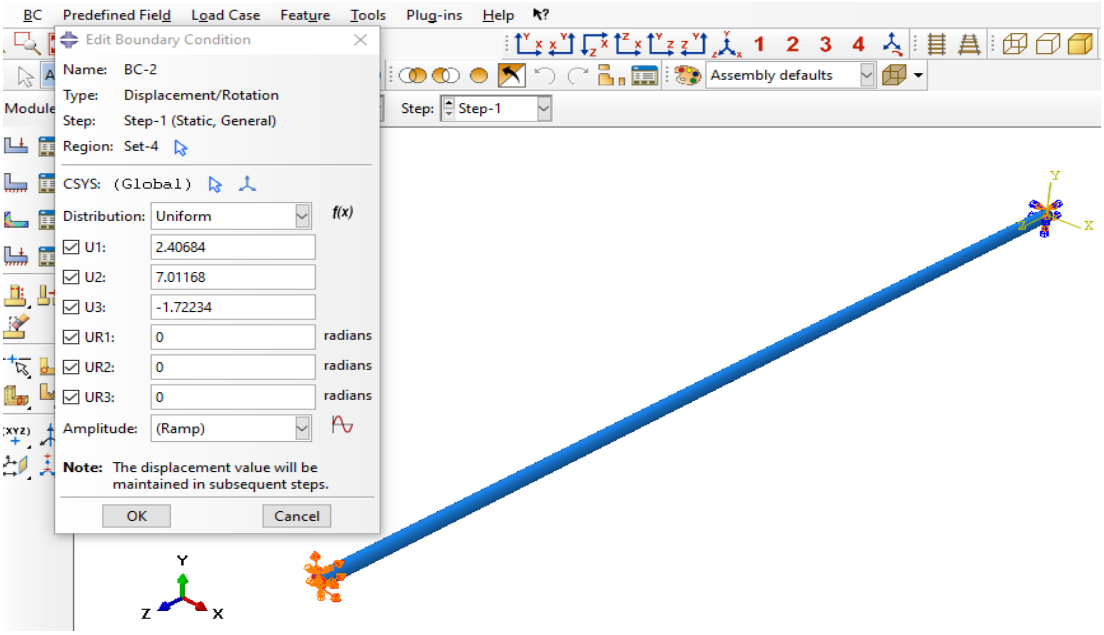

Figure 3.7: combined Fracture Mode I & III loading with initial crack

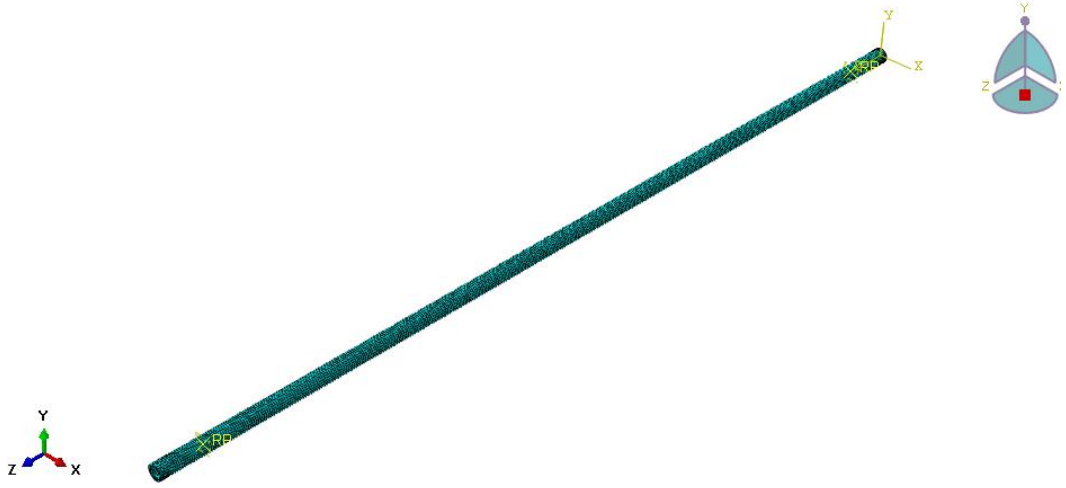

Figure 3.8: meshed cracked shaft for combined Mode I & III

For the contour integral

The crack depth for different crack length is presented in the following figure. The crack initiation used q vectors.

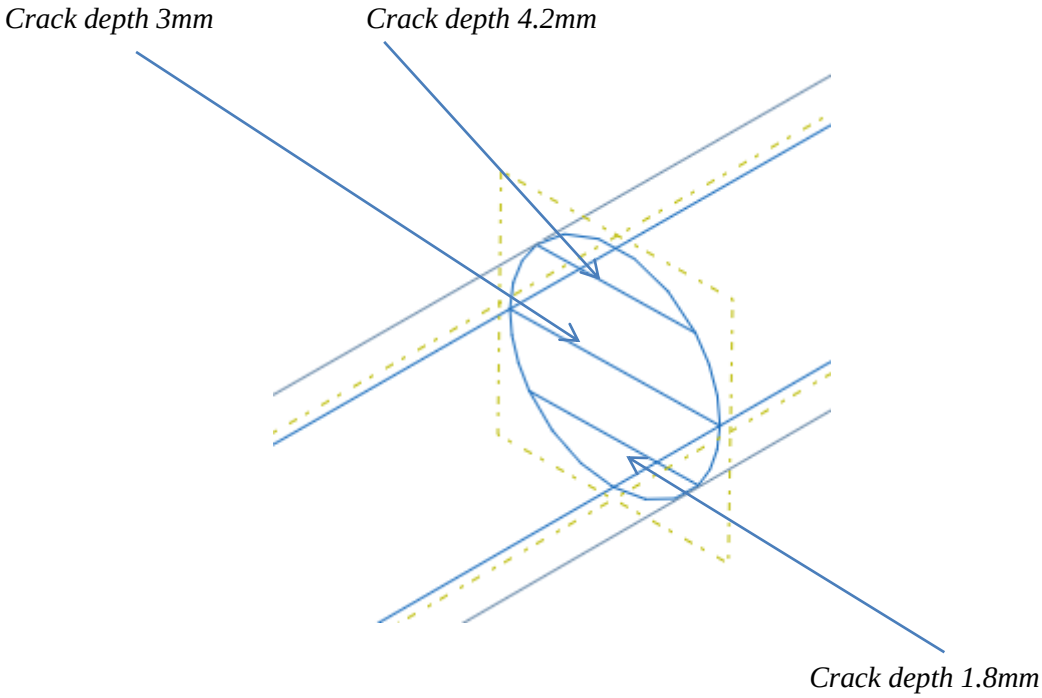

Figure 3.9: crack depth for contour crack initiation

Load

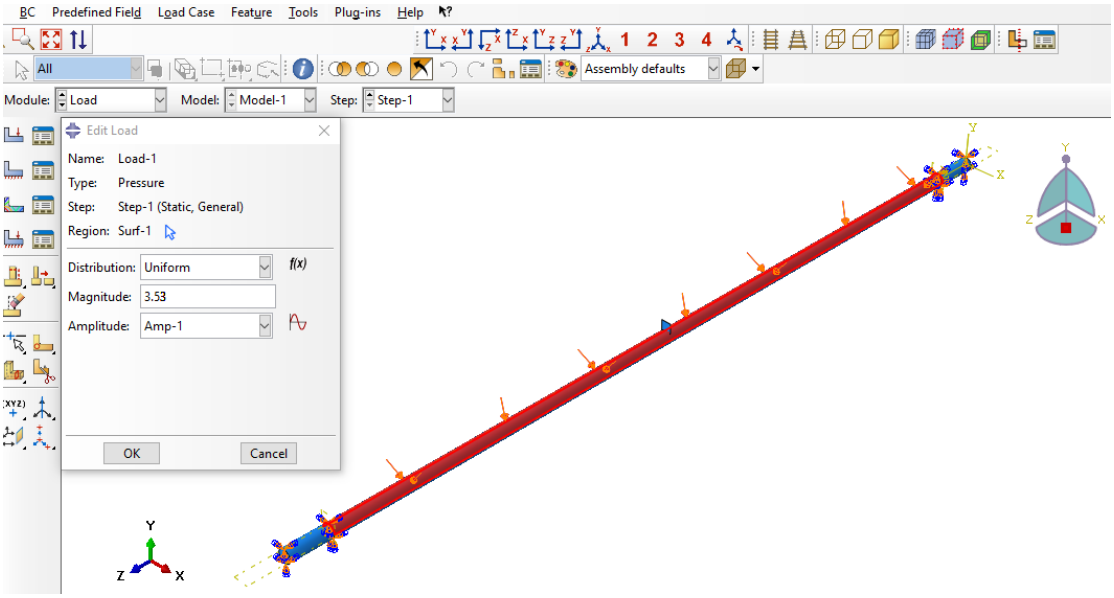

Figure 3.10: distributed load with two constrained ends

3.3. EXPERIMENTAL SETUP

Experimental Procedures

Apparatus

- ❖ Shafts with two discs
- ❖ Whirling machine

Before the whirling lab experiment, the purchased AISI 1018 rod was cut according to the required length. The lab procedures that were applied are the following.

1. 480mm length rod was mounted into the two bearings.
2. Then the two 1 Kg masses were arranged along the shaft.
3. The casing/cover was closed and tightened.
4. Push the safety button next.
5. Start the whirling machine.
6. Increase the speed gradually.
7. Hold when the shaft became unstable and increase the speed again.
8. Register/record the speed at the instability

Samples

The profile of each shaft is shown below.

Specimen I

Figure 3.11: shaft without crack

Specimen II

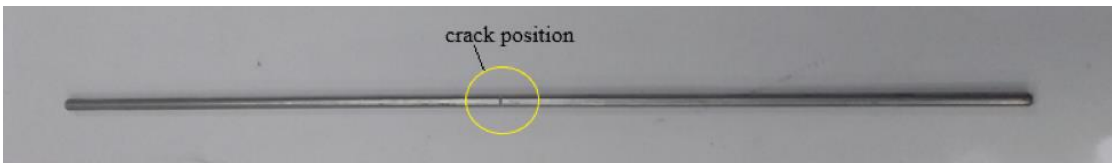

Figure 3.12: shaft with crack

CHAPTER IV

ANALYTICAL RESULTS

4.1. Material AISI 1018

1018 Mild Steel Alloy 1018 is the most commonly available of the cold-rolled steels. It is generally available in a round rod, square bar, and rectangle bar. It has a good combination of all of the typical traits of steel - strength, some ductility, and comparative ease of machining.

Table 1: properties of AISI 1018 [67]

1018 Mild (low-carbon) steel		
Minimum Properties	Ultimate Tensile Strength MPa	440
	Yield Strength, MPa	220
	Density	7850 Kg/m3
	Elongation	15.0%
	Rockwell Hardness	B71
	Hardness, Brinell (metric)	126
	Hardness, Rockwell B (metric)	71
Chemistry	Iron (Fe)	98.81-99.26%
	Carbon (C)	0.18%
	Manganese (Mn)	0.6-0.8%
	Phosphorus (P)	0.04% max
	Sulphur (S)	0.05% max

Table 2: Result of Tensile Test of AISI 1018 (5)

			Strength (Tensile)					
Number	Material	Condition	Yield S_y, MPa (kpsi)	Ultimate S_u, MPa (kpsi)	Fracture, σ_f, MPa (kpsi)	Coefficient σ_0, MPa (kpsi)	Strain Strength, Exponent m	Fracture Strain ϵ_f
1018	Steel	Annealed	220 (32.0)	341 (49.5)	628 (91.1)†	620 (90.0)	0.25	1.05

Assumption

1. Homogenous, isotropic AISI 1018 Steel shaft is used.
2. At the two supports, the displacement of the shaft is zero (the system is constrained at the two ends).

3. An arbitrary distance between the loads and the bearings are taken, since the research is only interested to find out the failure associated with critical speeds.
4. The crack dimension is too small. Therefore, it is negligible during critical speed calculation of the cracked shaft.
5. Eccentricity of the shaft during rotation is zero.

4.2. STRESS CALCULATION

It is not necessary to evaluate the stresses in a shaft at every point; a few potentially critical locations will suffice. Critical locations will usually be on the outer surface, at axial locations where the bending moment is large, where the torque is present, and where stress concentrations exist [5]. This helps us predict stress concentration points before the failure initiates.

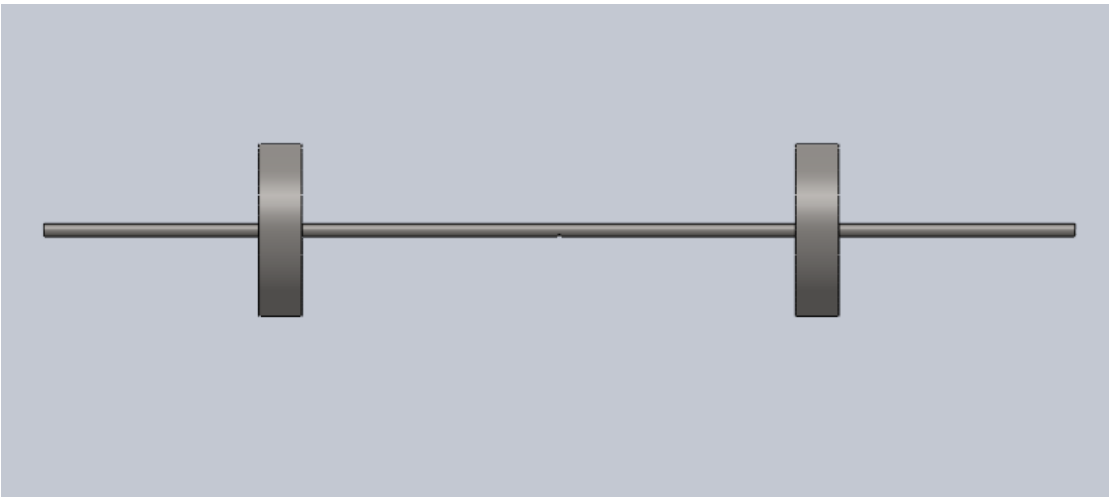

(a)

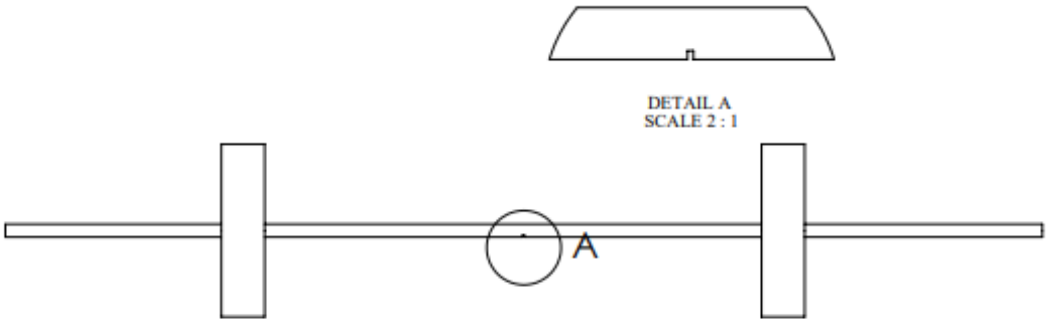

(b)

Figure 4.1: (a) the shaft (b) the shaft with two discs

From the provided specification the force could be calculated as the following:

$$F = mg = 1 * 9.81 = 9.81N$$

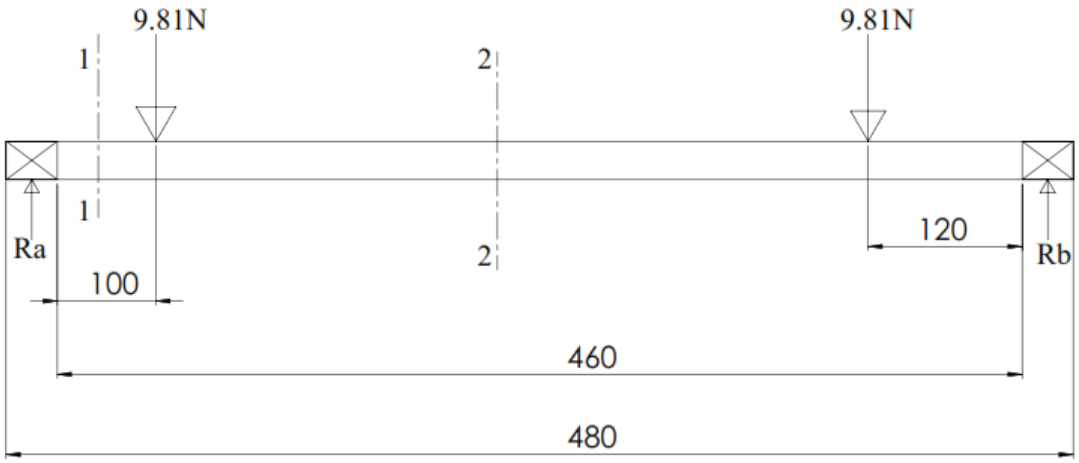

Figure 4.2: shaft loading

From statically equilibrium equation (SEE) the following was found:

$$+\uparrow \sum F = 0$$

$$\sum M = 0\ ccw$$

Thus,

$$\sum MB = 0\ ccw, \qquad R_A * 0.47 - 9.81 * 0.97 - 9.81 * 0.13 = 0$$

$$R_A = 10.44N$$

$$R_B = 9.18N$$

The moment at each section became:

Section- 1 $0 \leq x \leq 11$

$$\sum M_{CCW} = 0 - R_A * X + M$$

Then,

$$M = R_A * X$$

At X = 0.11m – M = 1.15Nm

Section-2 $11 \leq x \leq 35$

$$\sum M_{CCW} = 0$$

$$-R_A * X + 9.18(X - 0.11) + M = 0$$

$$M = R_A * X - 9.18(X - 0.11) = 1.44Nm$$

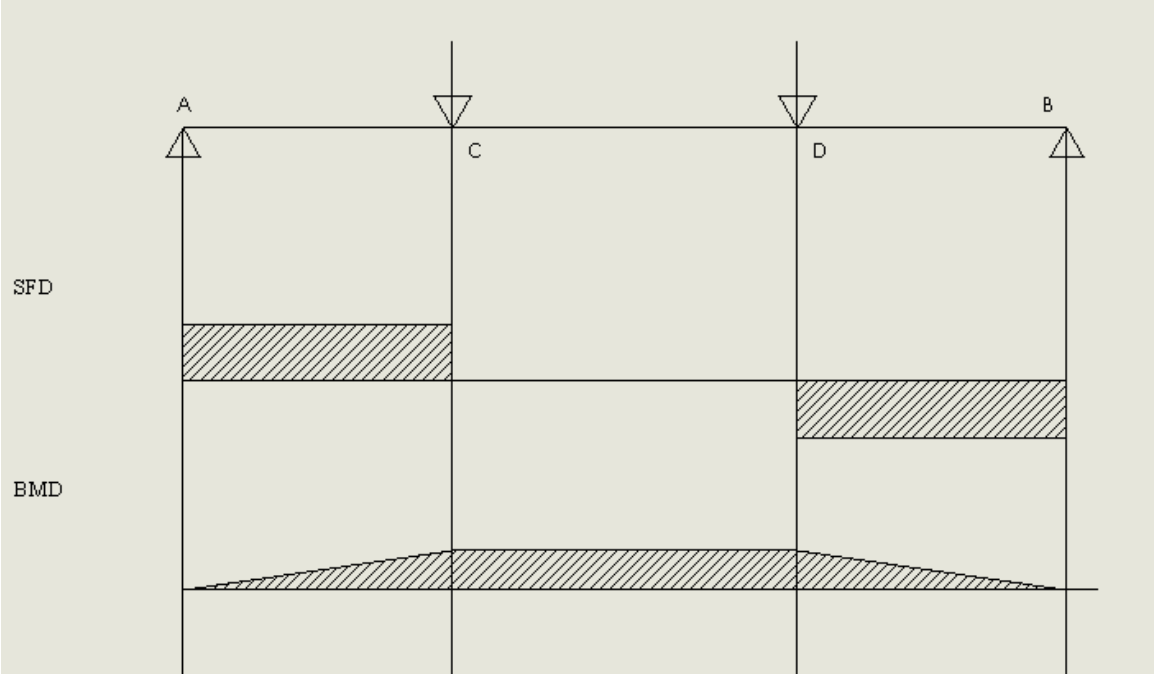

Figure 4.3: bending and shear force diagram

From the above diagram stress is concentrated at the point C and D. This depicts the potential failure could be associated with the bending and torsional load. Therefore, let's determine the reaction force first.

The bending stress becomes:

$$\sigma = \frac{Mc}{I}$$

$$I = \frac{\pi D^4}{64} = \frac{\pi * 0.006^4}{64} = 6.36 * 10^{-11} m^4$$

Thus,

$$\sigma = \frac{1.44 * 0.003}{6.36 * 10^{-11}} = 6.8 * 10^7 Pa$$

And the shear stress became the following

$$\tau = \frac{TR}{J}$$

$$J = \frac{\pi D^4}{32} = \frac{\pi * 0.006^4}{32} = 1.27 * 10^{-10} m^4$$

And from the output power and angular speed the torque was calculated as

$$\tau = \frac{P}{\omega} = \frac{370}{104.64} = 3.53 Nm$$

So,

$$\tau = \frac{3.53 * 0.003}{1.27 * 10^{-10}} = 8.35 * 10^7 Pa$$

The principal stress

$$\sigma_{1,2} = \frac{\sigma_X + \sigma_Y}{2} \pm \frac{1}{2}\sqrt{(\sigma_X - \sigma_Y)^2 + \tau^2}$$

$$\sigma_1 = \frac{6.8 * 10^7}{2} + \frac{1}{2}\sqrt{(6.8 * 10^7)^2 + (8.35 * 10^7)^2} = 7.6 * 10^7 Pa$$

4.3. CRITICAL SPEED CALCULATION

A shaft is regarded as an elastic body, which is assumed to be rotating about its undeformed centroidal line with rotational speed ω. The motion of the body is divided into the rigid body motion, which defines the rotating frame, and the small elastic motion relative to this frame.

There are several ways to estimate a rotor' analysis and measurement:

- Elementary beam-theory equation
- Finite-element analysis
- Impact response
- Identify resonance in a waterfall plot
- Curve-fit measured deflection
- Ramp up speed to ultimate failure

Using elementary beam calculation for an ensemble of attachments, Rayleigh's method for lumped masses gave:

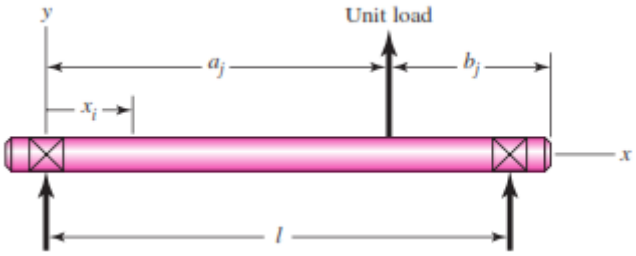

Figure 4.4: The influence coefficient δ_{ij} is the deflection at i due to a unit load at j [68]

$$\delta_{ij} = \begin{cases} \frac{b_j x_i}{6EIl}\left(l^2 - {b_j}^2 - {x_i}^2\right) & \text{for } x_i \le a_i \\ \frac{a_{i(l-x_i)}}{6EIl}(l^2 - {a_i}^2 - {x_i}^2) & \text{for } x_i \ge a_i \end{cases}$$

$$\delta_{11} = \frac{b_j x_i \left(l^2 - {b_j}^2 - {x_i}^2\right)}{6EIl} \quad for \;\; x_i \le a_i$$

$$\delta_{11} = \frac{0.11 * 0.36\ (0.48^2 - 0.11^2 - 0.36^2)}{6 * 2.1 * 10^{11} * 6.36 * 10^{-11} * 0.48} = 9.133 * 10^{-5} m$$

Due to Maxwell's reciprocity theorem $\delta_{12} = \delta_{21}$

$$\delta_{21} = \frac{0.11 * 0.13(0.48^2 - 0.11^2 - 0.13^2)}{6 * 2.1 * 10^{11} * 6.36 * 10^{-11} * 0.48} = 7.488 * 10^{-5} m$$

$$\delta_{22} = \frac{0.13 * 0.34(0.48^2 - 0.13^2 - 0.34^2)}{6 * 2.1 * 10^{11} * 6.36 * 10^{-11} * 0.48} = 1.125 * 10^{-4} m$$

The deflection became

$$y_1 = F_1\delta_{11} + F_2\delta_{12} = 10.44 * 9.133 * 10^{-5} + 9.18 * 7.488 * 10^{-5} = 1.64 * 10^{-3} m$$

$$y_2 = F_1\delta_{21} + F_2\delta_{22} = 10.44 * 1.125 * 10^{-4} + 9.18 * 7.488 * 10^{-5} = 1.86 * 10^{-3} m$$

Then, the critical speed using elementary beam theory was calculated as the following:

$${\omega_{11}}^2 = \frac{1}{m_1\delta_{11}}$$

$${\omega_{11}}^2 = \frac{1}{1 * 9.133 * 10^{-5}} = 104.64\ rad/s$$

$$\omega_{11} = 999.228\ rpm$$

And,

$$\omega_{22}{}^2 = \frac{1}{1 * 1.125 * 10^{-4}} = 94.28\, rad/s$$

$$\omega_{22} = 900.31\, rpm$$

Running the machine near or at the critical speed could lead to instability and damage if the shaft perpetually rotated at this point.

The natural frequency of the shaft was

$$\omega_1 = \left(\frac{\pi}{l}\right)^2 \sqrt{\frac{EI}{m}}$$

$$= \left(\frac{\pi}{0.5}\right)^2 \sqrt{\frac{2.1 * 10^{11} * 6.36 * 10^{-11}}{1}} = \frac{144.3m}{s} = 1377.76\, rpm$$

4.4. Finding Fracture Parameters

Previous studies indicated that, no significant decrease in shaft stiffness was observed for quasi-static loading of shafts containing closed dynamic cracks smaller than approximately 20% of shaft diameter, [68].Shallow cracks, which have a depth less than 25% of the shaft diameter, will not be able to stimulate the breathing effect. As such, the crack used in this study had a depth of 30% of the diameter along the radial direction of the specimen shaft.

The original crack length and the individual crack extensions are measured on the fracture surfaces.

Hence, the notch depth became,

$$\frac{a}{w} = 0.3 \;\; then\; a = 1.8\, mm$$

Table 3: Specification

Diameter of shaft (D)	6mm
Length of Shaft (L)	500mm
Notch depth (a)	1.8mm
Notch width (w)	6mm

Table 4: Fracture toughness of materials [69]

Material	$G_{Ic}(KJm^{-2})$	$K_{Ic}(MNm^{2})$	*E (GPa)*
Steel alloy	*107*	*150*	*210*

4.5. Stress Intensity Factor

For the analytic solution, the stress intensity factors K_I for Mode-I KIII for Mode-III could be calculated by using the equations given in [70].

For Mode-I (Opening Mode)

K_I was given for radial cracks around cylinders as follows:

$$K_I = \sigma_\infty \sqrt{\pi a}\left(\frac{D}{d} + \frac{1}{2} + \frac{3}{8}\frac{d}{D} - 0.36\frac{d^3}{d^3} + 0.73\frac{d^3}{D^3}\right)\frac{1}{2}\sqrt{\frac{D}{d}}$$

Where σ_∞ is the externally imposed tensile stress far from the crack,

$$\sigma_\infty = \sigma_{nom} = \sigma_A = 7.6 * 10^7 Pa$$

Where D is outer diameter of the shaft, d is crack tip diameter.

And after some calculations the value of K_I was,

$$K_I = 1540304 \text{ Pa}\sqrt{m}$$

Table 5: Calculation of Stress Intensity Factor for different crack depth

D (mm)	d (mm)	KI (Stress Intensity Factor) Pa$\sqrt{m}$
6	1.8	1540303.998
6	2.1	1260149.334
6	2.4	1064645.98
6	2.7	922371.0341
6	3	815629.1105
6	3.3	733776.7528
6	3.6	670072.1558
6	3.9	620063.382
6	4.2	580708.6045
6	4.5	549869.7495
6	4.8	526007.8458
6	5.1	507992.7012

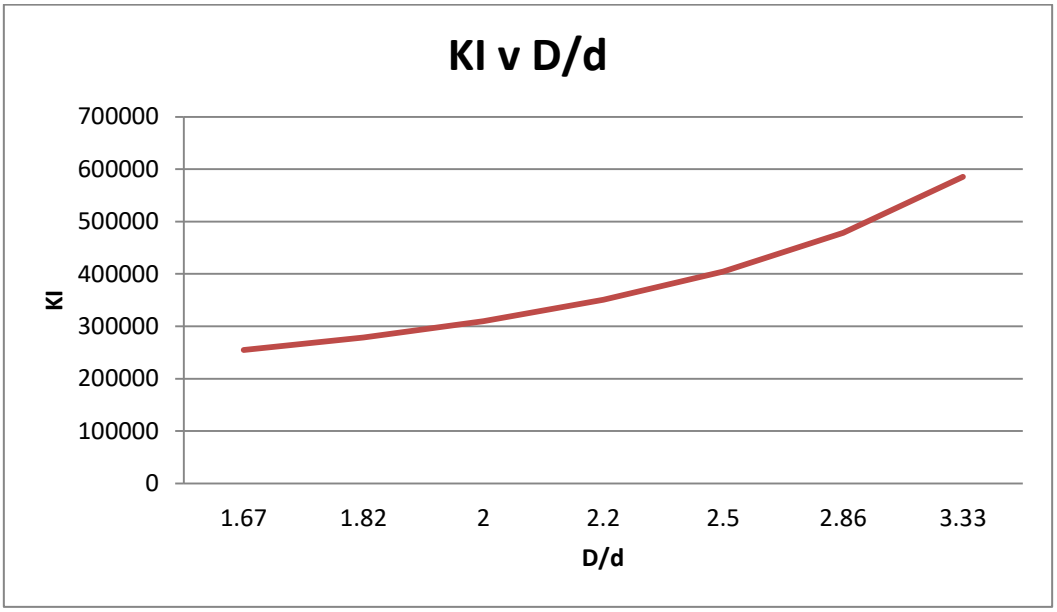

Figure 4.5: stress intensity factor versus D/d ratio

For Mode-III (Tearing Mode)

K_{III} is given for radial cracks around cylinders as follows

$$K_{III} = \tau\sqrt{\pi a}\left(\frac{D^2}{d^2} + \frac{1}{2}\frac{D}{d} + \frac{3}{8} + \frac{5}{16}\frac{d}{D} + \frac{35}{128}\frac{d^2}{D^2} + 0.21\frac{d^3}{D^3}\right)\frac{3}{8}\sqrt{\frac{D}{d}}$$

Where

$$\tau = \tau_{nom} = \tau_1 = 8.35 * 10^7 Pa$$

And after some calculations the value of K_{III} is,

$$K_{III} = 6787418 \text{ Pa}\sqrt{m}$$

Combined Mode I & III

The process zone criteria proposed by Radaj and Zhang also yield the general form of equation partly extended by the addition of linear K_I and K_{II} terms. The corresponding curves (σ_{1d} and τ_{1d} for 'ductile' behaviour, σ_{1b} for brittle behaviour) result from evaluating the crack propagation angle in the different mixed-mode (inclusive of single-mode) loading states. The following more conservative form, equation, is

$$K_{eq} = \sqrt{{K_I}^2 + {K_{II}}^2 + {K_{III}}^2} = 6959998.5\text{Pa}\sqrt{m}$$

4.6. Energy release rate

The most well-known equation of motion was obtained for a finite crack propagating in an infinite medium. In this case, the equation took the form [45]

$$\Gamma(v) = G(l,v) = \frac{{\sigma_\infty}^2}{E} l\left(1 - \frac{v}{C_R}\right)$$

Here *l* is the crack length, E is Young's modulus and C_R is the Rayleigh wave-speed. For Poisson's ratio = 0.3, the C_r/C_o= 0.57.

Where $C_O = \sqrt{El/\rho}$, the speed of sound for one-dimensional wave propagation.

$$C_o = \sqrt{\frac{El}{\rho}} = \sqrt{\frac{210 * 10^9 * 0.48}{7850}} = 3583.4\, m/s$$

Thus,

$$c_r = 0.57 * c_o = 2042.5\, m/s$$

Then

$$G(l,v) = \frac{\left(6.84 * 10^7\right)^2}{210 * 10^9} * 0.48\left(1 - \frac{0.3}{2042.5}\right) = 1.07 * 10^5\, J/m^2$$

4.7. Crack speed

The crack speed was given as:

$$V = c_r\left(1 - \frac{a_o}{a}\right)$$

Where w_f is the work of fracture, in the limit of an ideally brittle material, $w_f = \gamma_s$, the surface energy.

$$a_o = \frac{2Ew_f}{\pi\sigma^2}$$

Surface energy was calculated as:

$$\gamma = \frac{1540304^2}{2E} = \frac{2700^2}{2 * 210 * 10^9} = 0.564N/m$$

So,

$$a_o = \frac{2 * 210 * 10^9 * 0.564}{\pi(6.84 * 10^7)^2} = 1.61 * 10^{-4} m$$

Therefore, *V = 2040 m/s*

CHAPTER V

Numerical and Experimental Results and Discussion

5.1. SPECTRO-MAX RESULT

This test was used to know and check the homogeneity of the material. As we reckon defect and discontinuity in the material were a source of stress concentration area. And the material was found to be more or less similar throughout the cross-section. The result of SPECTRO-max data for each shaft was presented in the appendix.

The measured chemical composition corresponds in the tables of materials to steel with the prescribed chemical composition given in Table1.

5.2. Simulation Results and Analysis

Operating the shaft at a higher critical speed near to the natural frequency created excitation in the system that brought total damage to the shaft. And the result showed, for the shaft without initial crack, only bending or deflection occurred (where the speed was limited to 2700 rpm) as it was shown in figure 5.2. And the amplitude (in figure 5.1) of the shaft was constant during this second mode of whirling. However, the shaft with crack initiation failed at the second higher natural frequency.

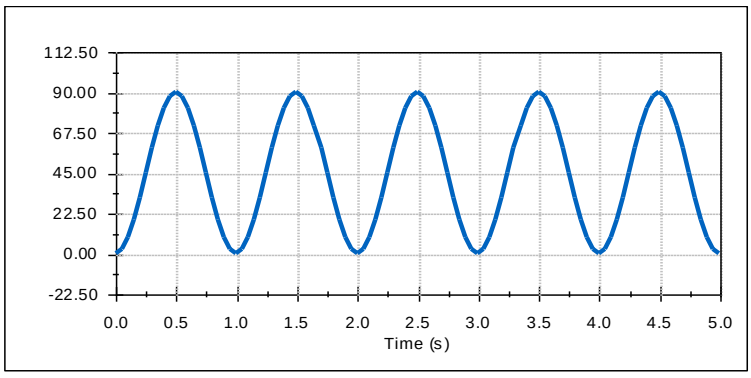

Figure 5.1: the amplitude of the whirling shaft

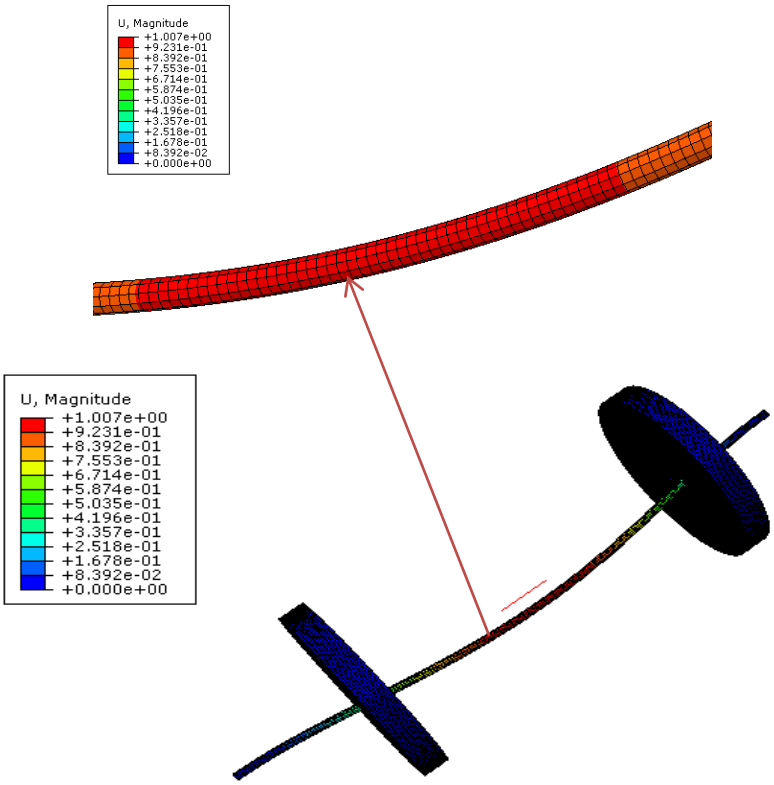

Figure 5.2: deflection of shaft without crack in mm

Abaqus/ Torsional simulation results with two concentrated load

The two loads brought the shaft to bend. The twisting effect on the shaft resulted in the dislocation of the shaft material. As it was shown in the figure 5.5 the displacement for un-deflected shaft material was unchanged but in the twisted shaft material the displacement varies.

The development of the twisting effect in the shaft increases as shown in the figure 5.3. The figure even told the material dislocation with twisting effect. The image of the displacements seemed squeezed or twisted object by itself which gave us the general picture of the torsional effect on the material (see also Appendix II).

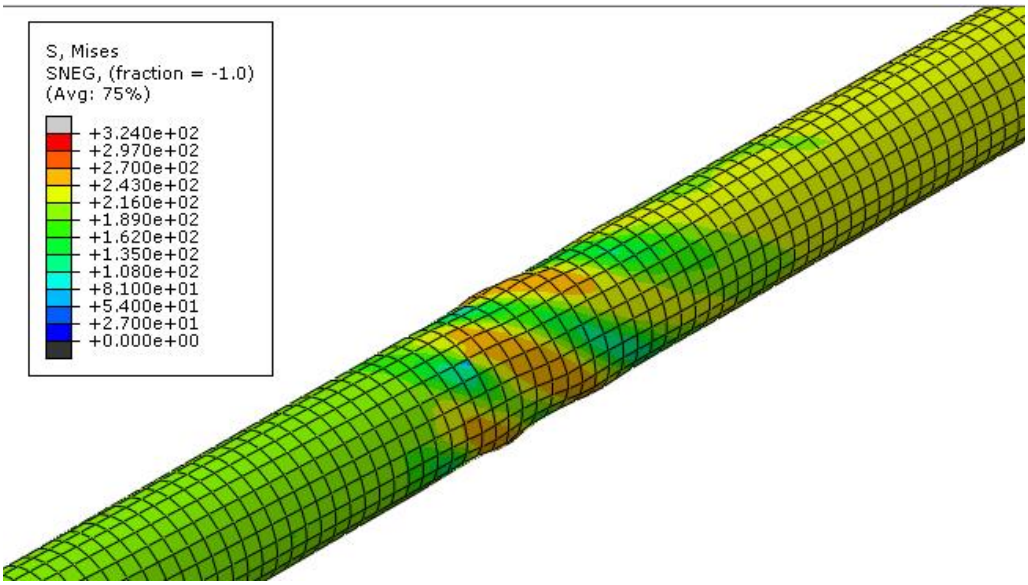
S, Mises
SNEG, (fraction = -1.0)
(Avg: 75%)
+3.240e+02
+2.970e+02
+2.700e+02
+2.430e+02
+2.160e+02
+1.890e+02
+1.620e+02
+1.350e+02
+1.080e+02
+8.100e+01
+5.400e+01
+2.700e+01
+0.000e+00

(a)

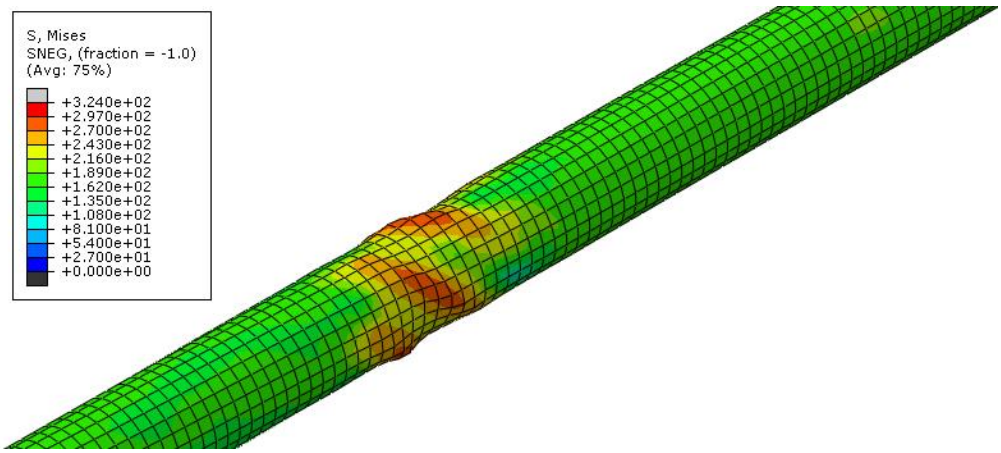
S, Mises
SNEG, (fraction = -1.0)
(Avg: 75%)
+3.240e+02
+2.970e+02
+2.700e+02
+2.430e+02
+2.160e+02
+1.890e+02
+1.620e+02
+1.350e+02
+1.080e+02
+8.100e+01
+5.400e+01
+2.700e+01
+0.000e+00

(b)

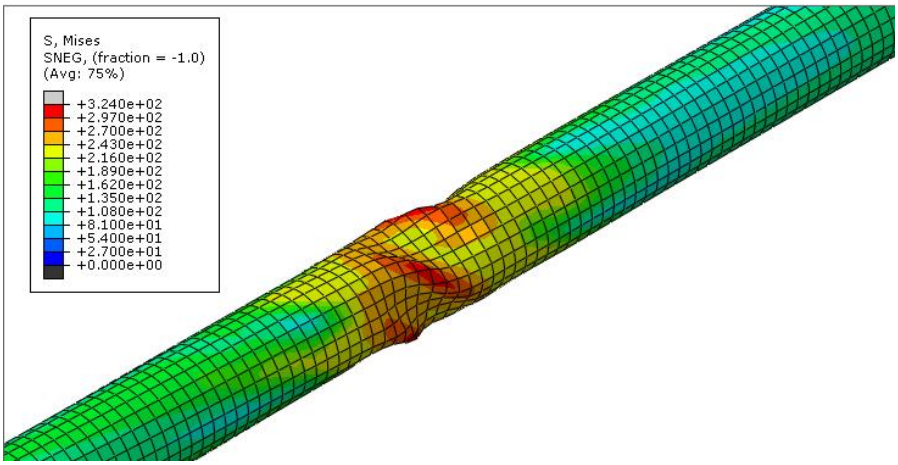
S, Mises
SNEG, (fraction = -1.0)
(Avg: 75%)
+3.240e+02
+2.970e+02
+2.700e+02
+2.430e+02
+2.160e+02
+1.890e+02
+1.620e+02
+1.350e+02
+1.080e+02
+8.100e+01
+5.400e+01
+2.700e+01
+0.000e+00

(c)

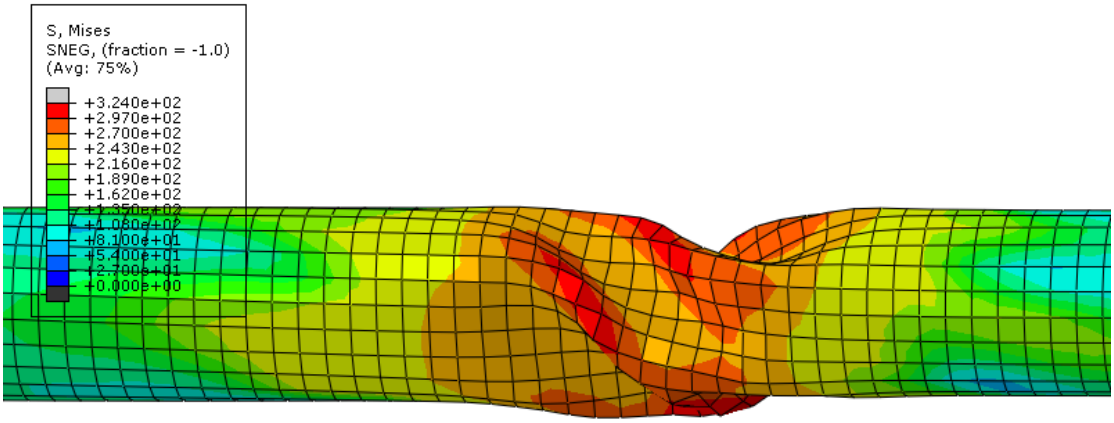

(d)

Figure 5.3 a, b, c & d Mode III twisting failure (S_Mises in Pa)

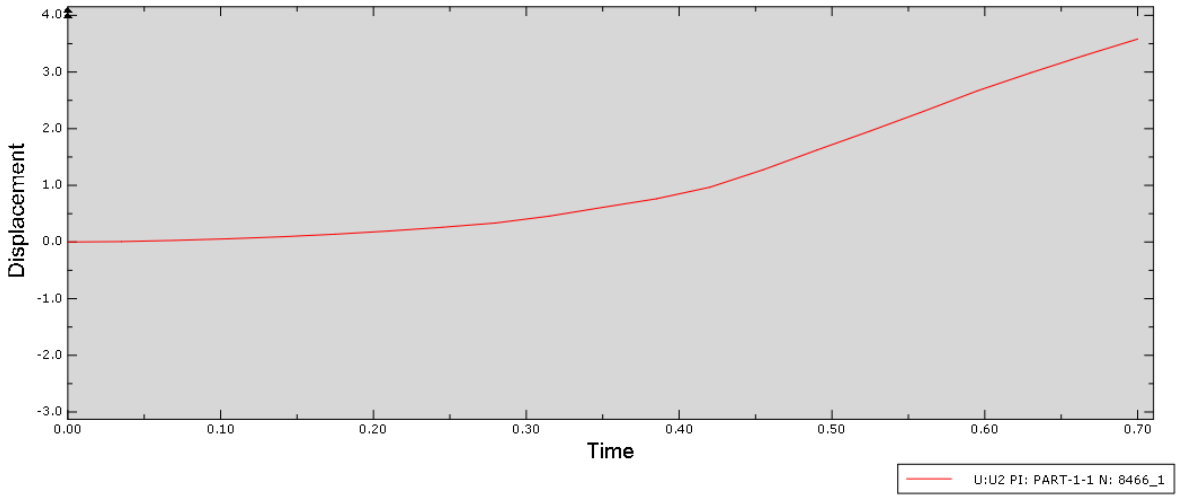

Figure 5.4: U: U2 PI: PART-1-1 N: 8336 From Field Data: U:U2 at part instance PART-1-1 node 8466 in (displacement in mm)

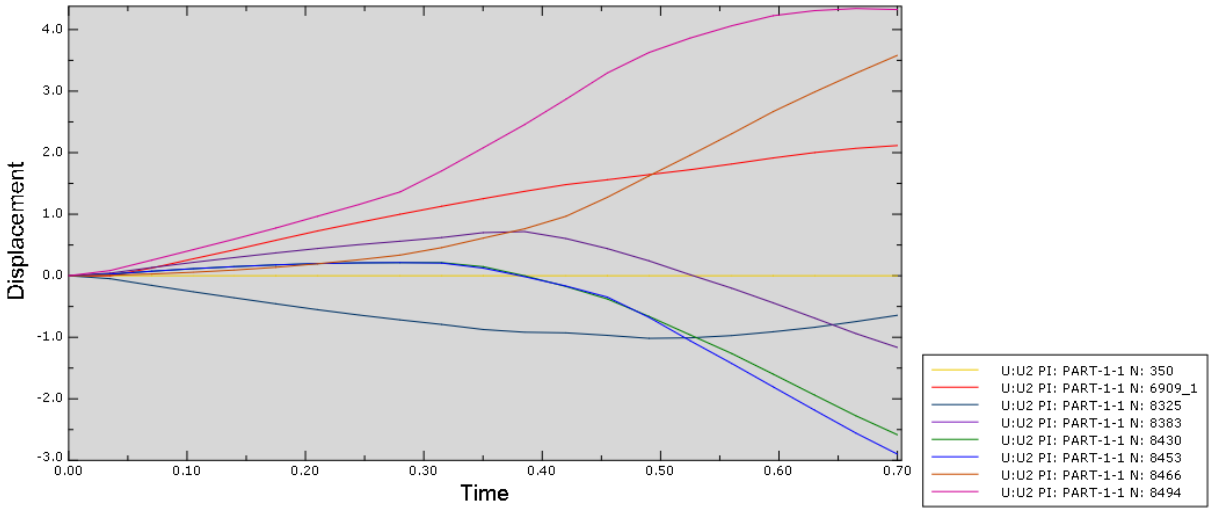

Figure 5.5: displacement for 8 nodes in mm

Abaqus/XFEM crack for combined mode

Crack Growth

The shaft crack was induced by nonsynchronous resonance. The existence of a crack in the shaft induces a reduction in the stiffness of the shaft which result necking (figure 5.17). As we can see in figure 5.17, the dark spot was the place where the crack initiates. And it perpetually grew till the end (figure 5.6 to 5.9).

Failure occurred when the material that had not been affected by the crack could not withstand the applied loads any longer in this case it means the shaft could not resist both the rotational speed (figure 5.3) and the 1 Kg loads applied to it. As the crack propagates the stress increases continuously till the final fracture.

Since the applied load was a catastrophe (impact) load, the failure occurred very rapidly once the crack reached yielding.

Since there was an initial opening, the crack type that causes the failure was transversal crack. Generally, cracks propagated in surfaces which were roughly planar and perpendicular to the rotating axis of the shaft. And from observation and result, the crack mode was a combination of Mode I and III.

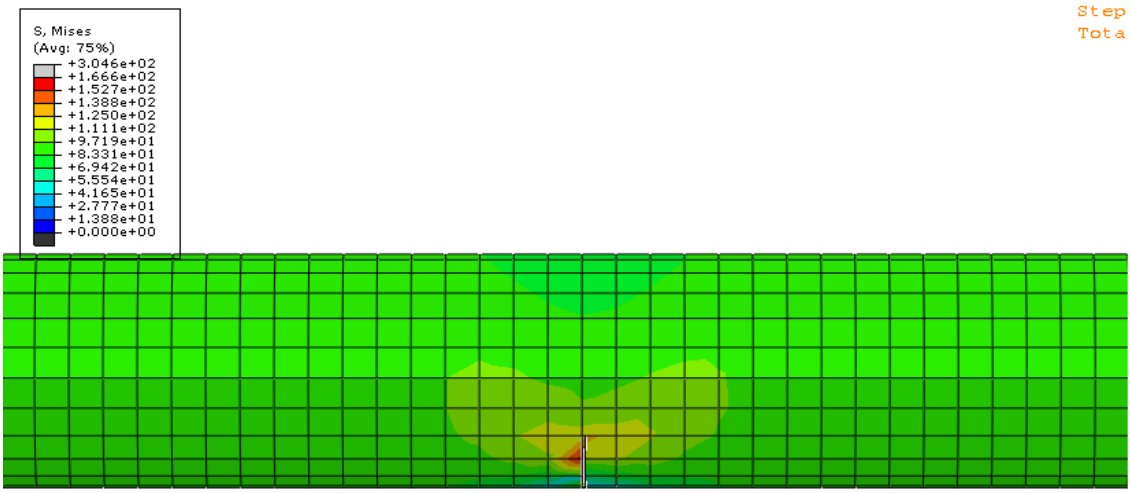

Figure 5.6: Crack in the shaft with an initial crack opening (Combined Mode I & III) (S_Mises in Pa)

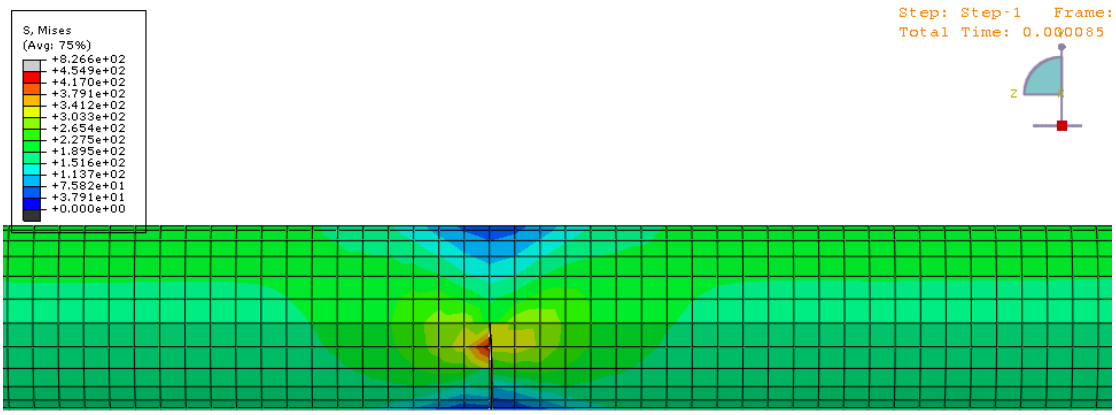

(a)

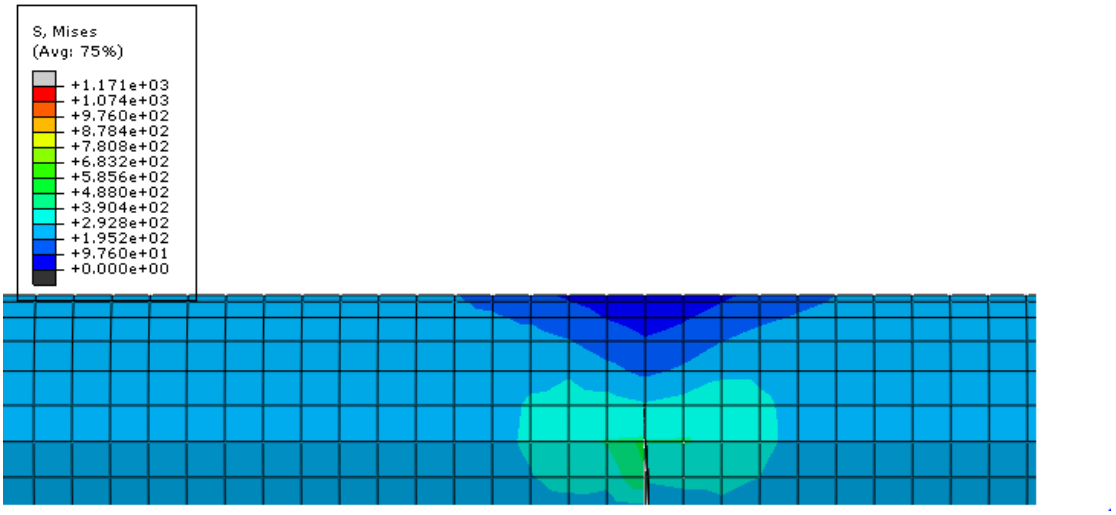

(b)

Figure 5.7: (a) & (b) Crack propagation in the shaft (Combined Mode I & III) (S_Mises in Pa)

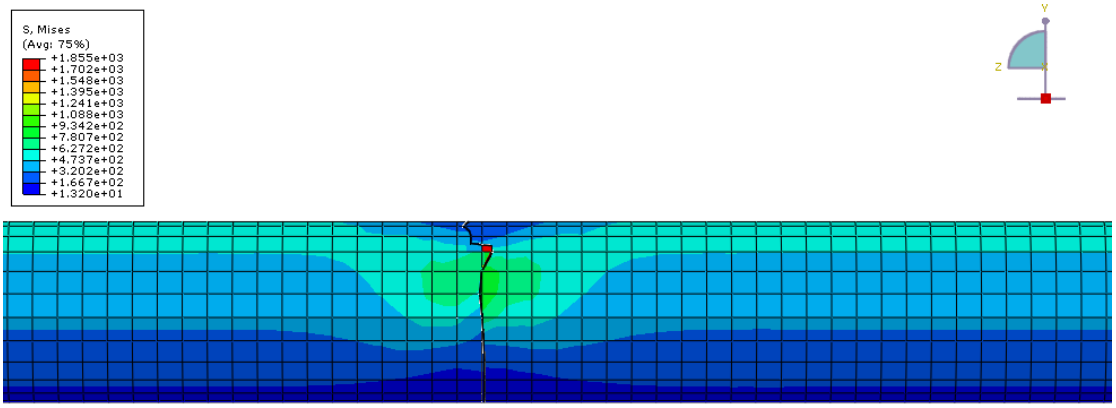

Figure 5.8: Crack growth propagation in the shaft (Combined Mode I & III) (S_Mises in Pa)

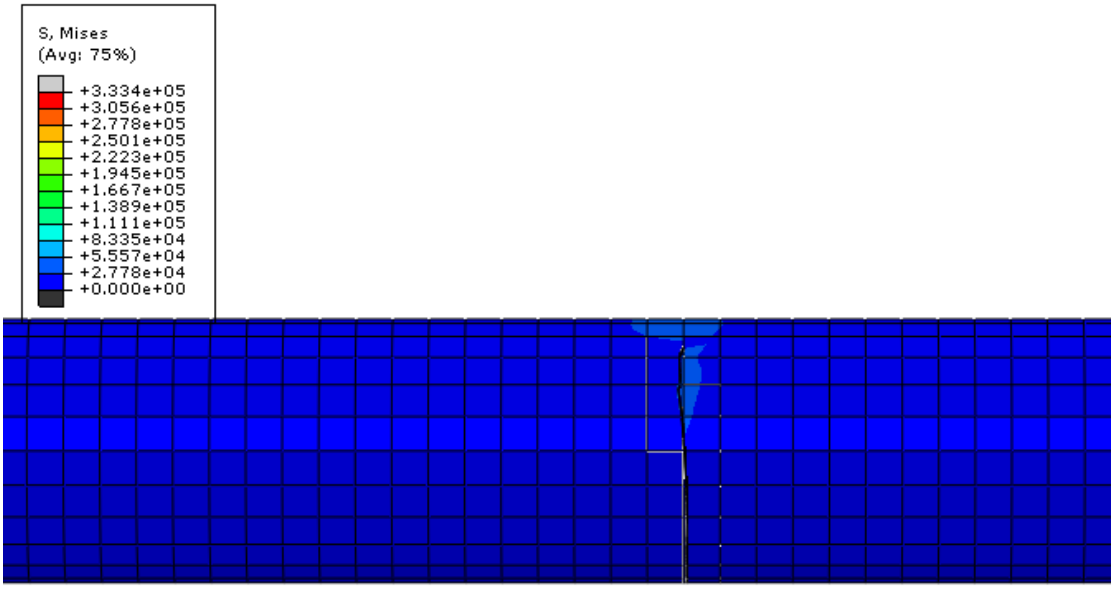

Figure 5.9: Final Fracture in the shaft (S_Mises in Pa)

Figure 5.10 indicates that the strain energy release rate showed locally highest pitch value after yielding of the specimen and progressively decreasing as the crack increases. Usually, the plane stress condition was applied for a thin elastic problem and the plane strain condition was for an infinite case. The Strain Energy Release Rate (SERR) for plane stress was larger than plane strain. Through the figure below, we could observe the transition of local yielding condition. The energy release rate showed relatively higher value for 0.05 seconds. Then, as the time was increased, the energy release rate was getting lower until the final fracture happened.

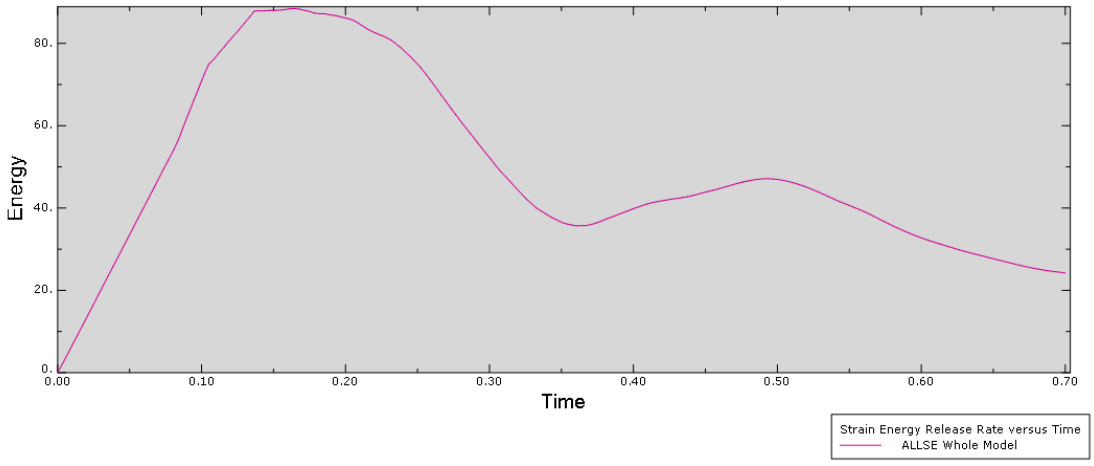

Figure 5.10: Strain Energy Release Rate versus time graph in KJ/m^2

Abaqus/Countour Inegral Results

First, different depths were introduced to investigate the 3D effect along the crack line. It could be expected for the depth expansion to give an effect on the SERRs along the crack line since the variation of boundary condition corresponding to position along the depth would affect the effective modulus and stress. For this numerical model, the length (L) was fixed as 480 mm.

Results found using contour integral showed the crack propagation at different crack depth. And the strain energy versus time graph varies according to the predefined crack depth. The one shown in the figure 5.16 was the highest value found.

The strain energy release rate versus time graph showed that the crack depth had a significant effect on the value of strain energy release rate. For the first two crack depth the value was more or less similar (figure 5.12 & 5.14). But for last one it went up to 500 MJ/m^2. Finally, we can observe that the energy release rate drops dramatically at the free surface after yielding. But here the plastic region is relatively wider than the one found in the XFEM.

Comparing this result with the one simulated with XFEM, it was found that the XFEM result (figure 5.10) was more or less similar with the first two values of contour integral and less than the maximum crack depth strain energy release rate value.

Overall the stress intensity factor of the simulation result was a bit lower than the manual calculated value.

For instance for the first crack depth, which was 1.8mm, the manual calculation result was

$K_I = 1540304\ \text{Pa}\sqrt{m}$

$K_{III} = 6787418\ \text{Pa}\sqrt{m}$

And the Abaqus result was

H-OUTPUT-1_CRACK-1

-1-	K1:	1.4626E+06
	K3:	6.4497E+05

Therefore, the Abaqus results was the most reliable one in this case. Because it considered the removed crack area.

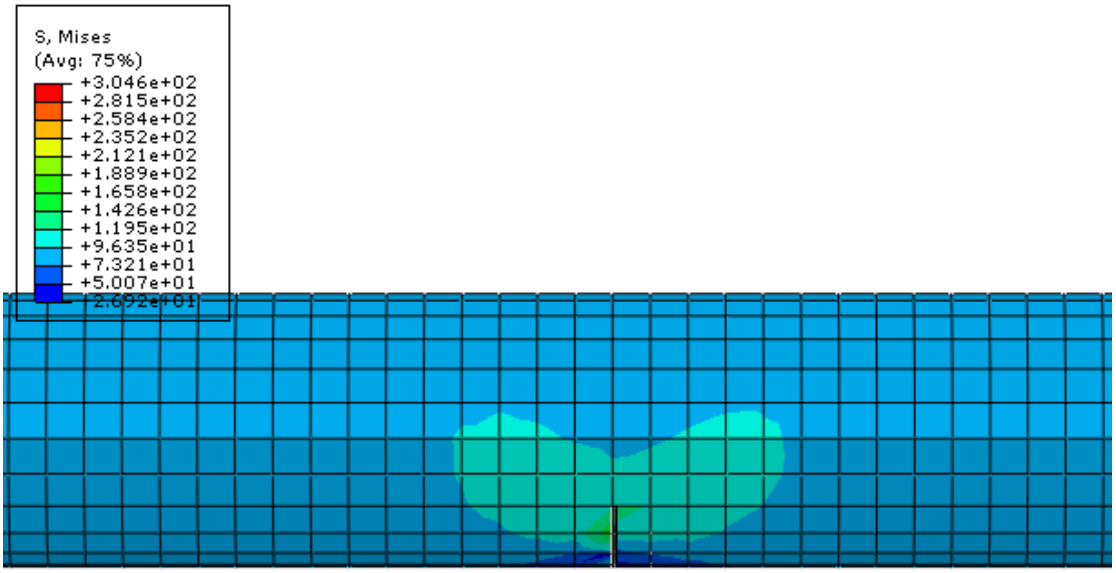

Figure 5.11: crack growth in shaft with initial crack depth of1.8mm using contour integral(S_Mises in Pa)

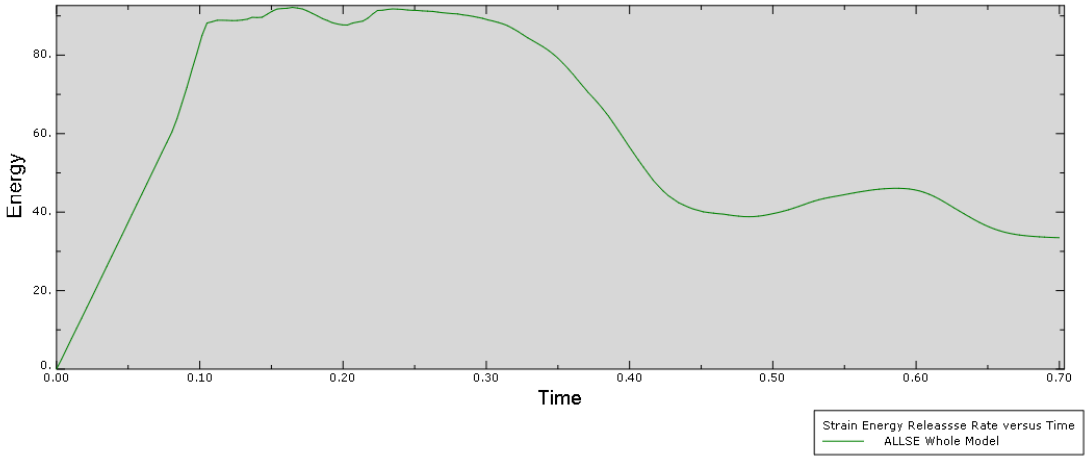

Figure 5.12: Strain Energy Release Rate versus time graph in KJ/m^2

H-OUTPUT-1_CRACK-2

-2- K1: 8.0924E+05

K3: 1.0897E+04

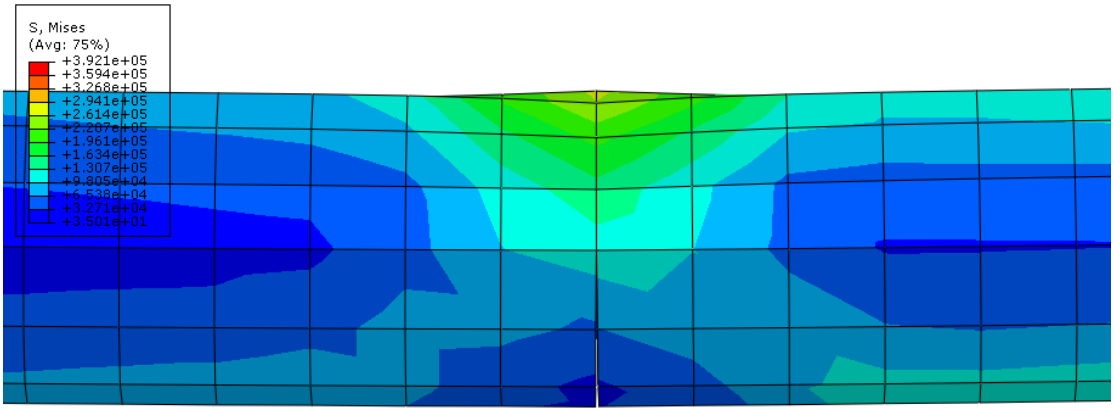

Figure 5.13: crack growth in shaft with initial crack depth of 3mm using contour integral (S_Mises in Pa)

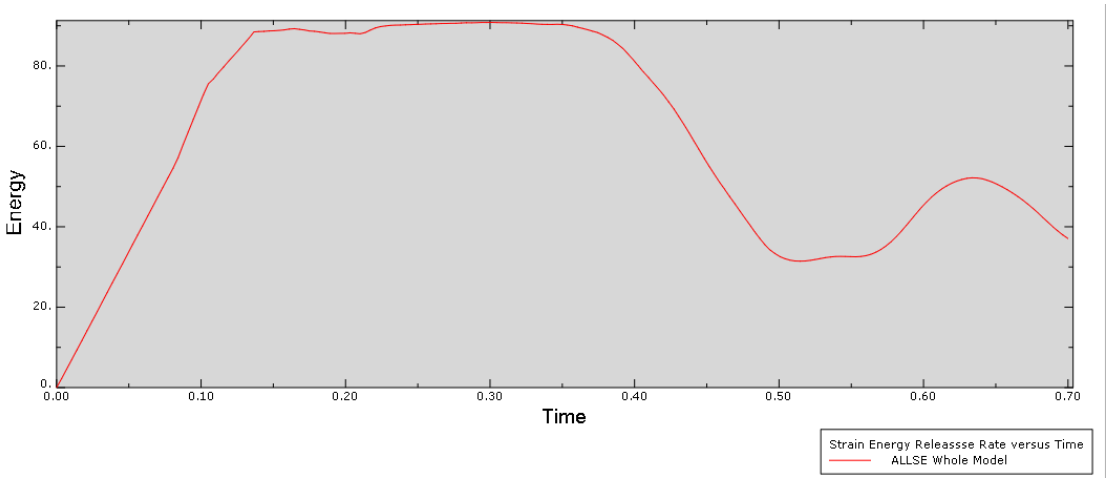

Figure 5.14: Strain Energy Release Rate versus time graph in KJ/m^2

H-OUTPUT-1_CRACK-3

-3- K1: 5.1798E+05

K3: 5.7482E+04

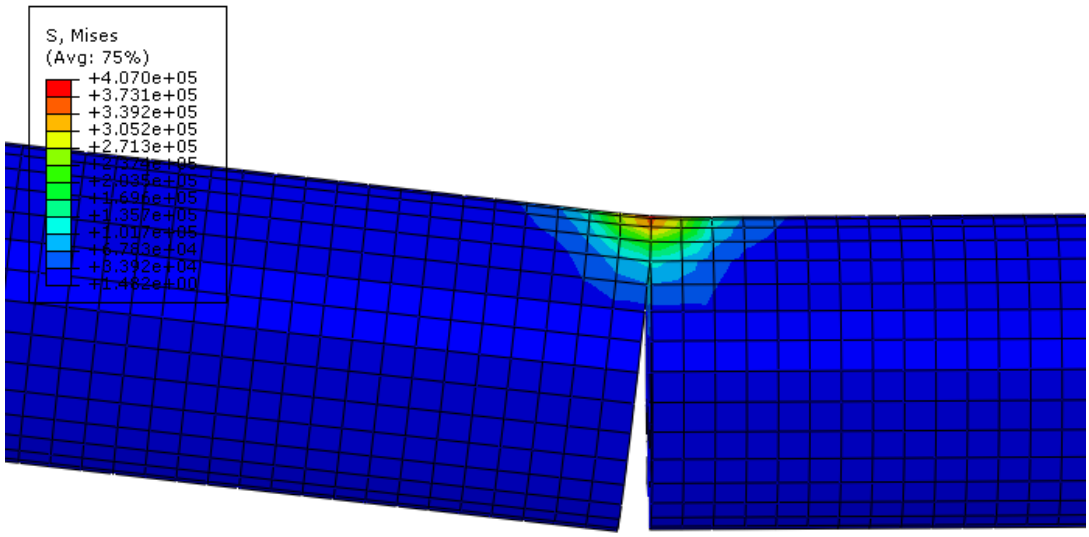

Figure 5.15: crack growth in shaft with initial crack depth of 4.2mm using contour integral (S_Mises in Pa)

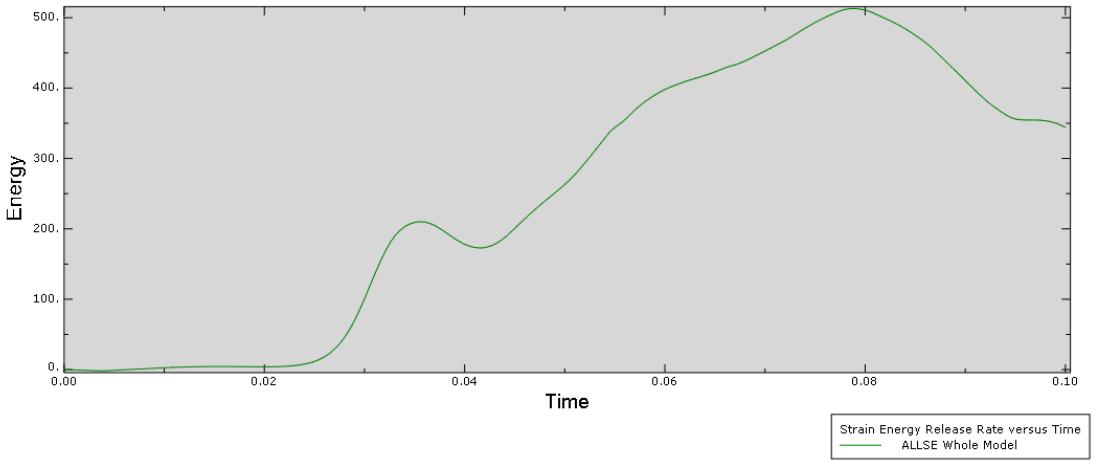

Figure 5.16: Strain Energy Release Rate versus time graph in KJ/m^2

5.3. Experimental Results and Analysis

Experiment one

Generally, the experiment followed steps that were put forward in the chapter three. The shaft run at different critical speed, the first critical speed was 890 rpm and the others were summarized below.

Table 6: Results found for specimen I

The first critical speed	890 rpm
The second critical speed	989rpm
The third critical speed	1355 rpm

The first and second critical speed differed from the numerical calculated value by 10 rpm.

The error was calculated as

$$\%\ error = \frac{|accepted(theoretical)value - experimental\ value|}{accepted\ value}$$

$$\%\ error = \frac{900.31 - 890}{900.31} * 100 = 1.15\% \quad and$$

$$\%\ error = \frac{999.228 - 989}{999.228} * 100 = 1.02\%$$

The error was negligible since it was too small.

Experiment two

The shaft with initial crack was found to fail near the second higher critical speed.

Table 7: Results found for specimen II

The first critical speed	820 rpm
The second critical speed	930 rpm
The third critical speed	1292 rpm

Of this experiment, the first critical speed differed from the experimental value by 80 rpm and the second varied by 70 rpm. Here there was a pronounced difference in experimental and theoretical calculation of critical speed due to the crack introduced. This result complied with different researches [25; 42] that had done before.

The error was calculated as

$$\%\, error = \frac{900.31 - 820}{900.31} * 100 = 8.92\% \quad and$$

$$\%\, error = \frac{999.228 - 930}{999.228} * 100 = 6.93\%$$

The percentage was large due to the decrease in critical speed.

ANALYSIS

In the first experiment, the shafts run at the second critical speed for 20 minutes. Near and at the critical speed, the shaft became unstable. And there was unpleasant noise. The shaft continued to whirl at those speeds. Finally, the shaft deflected and the machine stopped by itself. It showed that the shaft without an initial crack (ignoring other defects) deflected at the second higher critical speed.

During the second experiment, a high shocking sound appeared at the first critical speed. The bearing with the mass at the left went loosening twice. As it was evidenced by different researchers, it was common for various machine parts to go flying during resonance. If it was not for the casing, this might harm the experimenter. Here, at the second higher critical speed the shaft failed. As it was presented in the

figure 5.10, the cracked shaft failed due to resonance. Here initial necking was formed in the material before total failure of the rotor.

Result Summary

Table 8: Result summary

Sample	Length (mm)	Diameter (mm)	Critical Speed I (rpm)	Critical Speed II (rpm)	Natural Frequency (rpm)
A (cal)	480	6	900.31	999.228	1377.76
A (lab)	480	6	890	989	1355
B (cal)	480	6	900.31	999.228	1377.76
B (lab)	480	6	820	930	1292

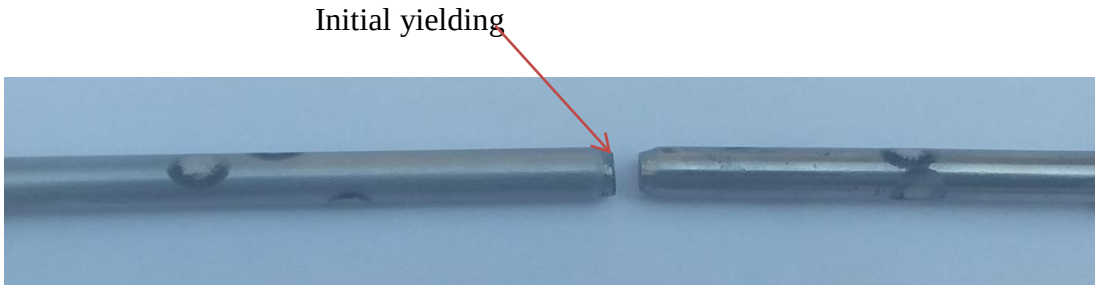

(a)

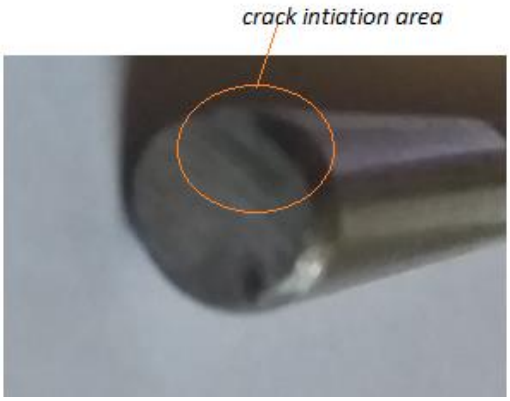

(b)

Figure 5.17: Experimental results

5.4. Limitation

The samples were taken only for steel shaft AISI 1018 that narrows the research extensively. It would be fine if there were several materials to be experimented with to reckon the crack mode to have a database. All in all the research tried to see one type of material to devise a general picture of the actual fracture of the shaft.

Again, the operating speed of the machine was a hindrance to find the third, fourth and other higher critical speed. Moreover, the vibration produced must be dumped to create a safe environment.

The last one was the availability of Scanning Electron Microscopy. It was hard to get a functional SEM machine to see and present the microstructure of the material.

CHAPTER VI

6.1. Conclusion and Recommendation

Natural frequency and critical speed of the shaft carrying two discs were found out theoretically and experimentally.

The critical speed of the shaft that was found during the experiment was a little bit smaller than the numerical calculated value. During experiment, the instability of the shaft started early before the sign of the first calculated numerical value.

The simulation result showed around 1mm value of deflection on the shaft without crack occurred at the second higher critical speed. However, in the experiment, the shaft deflected up to 3mm. So it seeks another consecutive and intensive experiment to see that much deflection. The research speculates the cycle of the operation or other defects might affect the deflection of the shaft.

The shaft with initial crack failed when the shaft run at the second higher critical speed. The experimental result confirmed the same. The crack began at the second higher critical speed. Generally, different evidence and literature shows there was shaft crack due to higher critical speed, so this research analyzed the failure of the shaft due to higher critical speed.

The research recommended the material for the high-speed shaft must be advanced in the future to avoid such failure or create a shaft that can move at a high speed.

6.2. Future work

The paper deemed further investigation must be done to compare this result with other materials to prepare a database for a various materials. Generally, the following could be considered as a future work.

- The effect of the distance between the two discs and the bearings
- The influence of the load size
- Fracture analysis of shaft failure due higher critical speed for different material

References

1. **Roylance, David.** *Introduction to Fracture Mechanics.* s.l. : Department of Materials Science and Engineering Massachusetts Institute of Technology Cambridge, 2001. MA 02139.

2. **Shipley, William T. Becker and Roch J.** *Failure Analysis and Prevention.* Ohio : ASM International, 2012.

3. **Collins, J.A.** *Failure of materials in mechanical design: analysis, prediction, prevention, 2nd ed.* New York : Wiley, 1993.

4. **Deepan Marudachalam M.G, K.Kanthavel, R.Krishnaraj.** *Optimization of shaft design under fatigue loading using Goodman method.* s.l. : International Journal of Scientific & Engineering Research, August-2011. Vol. Volume 2. ISSN 2229.

5. **Shigley, Richard G. Budynas and J. Keith Nisbett.** *Mechanical Engineering.* New York : The McGraw-Hill Companies, 2011.

6. **Haji, Zyad Nawaf.** *Dynamic Analysis and Crack Detection in Stationary and Rotating Shafts, School.* s.l. : Aerospace and Civil Engineering The University of Manchester, 2015. 2015.

7. **Dimarogonas, D.** *Vibration of cracked structures.* s.l. : A state of the art review. Engineering Fracture Mechanics, 1996.

8. **Nguyen, Saber El Arem and Quoc Son.** *Nonlinear dynamics of a rotating shaft with a breathing crack.* s.l. : Annals of Solid and Structural Mechanics, 2011.

9. **P. TREBUŇA, M. PÁSTOR, F. TREBUŇA, F. ŠIMČÁK.** *THE ANALYS IS OF FAILURE CAUSES OF THE ROTOR SHAFT OF STEAM TURBINES.* s.l. : METALURGIJA, 2017. ISSN 0543-5846.

10. **Berry, Holly.** *WHIRLING OF SHAFTS.* s.l. : www.freestudy.uk.co.

11. **Lissenden, C. J., Tissot, S. P., Trethewey, M. W., and Maynard, K. P.** *Torsion response of a cracked stainless steel shaft.* 2007.

12. **Robert G. Loewy and Vincent J. Piarulli.** *Dynamics of Rotating Shafts.* 1969 : The Shock and Vibration Information Center United States Department of Defence.

13. **Rao, Singirsu S.** *Mechanical Vibrations university of Miami.* s.l. : university of Miami, 2011. ISBN.

14. **Takle, Mr. Balasaheb Keshav.** *Experimental Investigation of Shafts on Whirling of Shaft Apparatus.* s.l. : International Journal of Science, Engineering and Technology Research (IJSETR), 8th August 2014. Vol. Volume 3.

15. **N. Lenin Rakesh, V. Palanisamy and S. Jeevabharathi.** *Stress Analysis of a Shaft Using Ansys.* s.l. : Middle-East Journal of Scientific Research, 2012. ISSN 1990-9233.

16. **AKPOBI, J.A. OVUWORIE.** *Computer–Aided Design of the Critical Speed of Shafts.* s.l. : JASEM, 2008. Vols. Vol. 12(4) 79 – 86. ASEM ISSN 11198362.

17. **Boudet, J. F., Ciliberto, S., and Steinberg, V.** *Crack dynamics in elastic media.* Paris : s.n., 1996.

18. **Fineberg, J., Gross, S. P., Marder, M., and Swinney, H. L.** *Instability in the propagation of fast cracks.* s.l. : Phys. Rev, 1992.

19. **Steven P. Gross, Jay Fineberg, M. Marder, W. D. McCormick, and Harry L. Swinney.** *Acoustic emissions from rapidly moving cracks.* s.l. : Phys. Rev. Lett., 1993.

20. **SteveGross, M.Marder and.** *Origin of crack tip instabilities.* s.l. : Journal of the Mechanics and Physics of Solids, 1995. Vol. Volume 43.

21. **Huang, S. S., Wu, M. C.** *In-Plane vibration and crack detection of a rotating shaft disk containing a transverse crack.* s.l. : Journal of Vibration and Acoustics, 1998.

22. **Grabowski, B.** *he Vibrational Behavior of a Turbine Rotor Containing a Transverse Crack.* s.l. : Transactions of the ASM, 1980.

23. **Khangar1, V. S.** *A Review of Various Methodologies Used for Shaft Failure.* s.l. : International Journal of Emerging Technology and Advanced Engineering, 2012. (ISSN 2250-2459.

24. **Sekhar, A.** *Crack identification in a rotor system a model-based approach.* s.l. : Journal of Sound and Vibration, 2004.

25. **P. Pennacchi, N. Bachschmid.** *A model-based identification method of ransverse cracks in rotating shafts suitable for industrial machines.* s.l. : Mechanical Systems and Signal Processing, 2006.

26. **Gasch, R.** *A survey of the dynamic behaviour of a simple rotating shaft with a transverse crack.* s.l. : Journal of Sound and Vibration, 1993.

27. **Chen, C., Dai, L., and Fu.** *Nonlinear response and dynamic stability of a cracked rotor.* s.l. : Communications in Nonlinear Science and Numerical Simulation, 2006.

28. **Henry, T., and Okah.** *Vibration in cracked shafts.* s.l. : Conference on Vibrations in Rotating Machinery, 1976.

29. **CASANOVA, FERNANDO.** *FAILURE ANALYSIS AND REDESIGN OF A WAGON WHEEL SHAFT FOR SUGAR CANE TRANSPORT.* s.l. : Universidad del Valle, 2010.

30. **Lai, R. K. C. Chan and T. C.** *Digital simulation.* s.l. : The Hong Kong Polytechnic University, Hong Kong, 1995.

31. **J.M. Vance, B.T. Murphy and H.A. Tripp.** *Critical Speeds of Turbo machinery.* New York : American Society of Mechanical Engineers, 1985.

32. **Wagner, E. R., Holzinger, D. W., and Nagele, F. C.** *Universal Joint and Driveshaft Design Manual, Advances in Engineering Series. No. 7.* s.l. : The Society of Automotive Engineers, 1991. ISBN 089883-007-9.

33. **Darpe, T. H. Patel and A. K.** *Influence of crack breathing model on nonlinear dynamics of a cracked rotor.* s.l. : Journal of Sound and Vibration, 2008. Vol. vol. 311.

34. **White, Robert J.** *Measurement Techniques for Estimating Critical Speed of Drivelines.* Waterloo, Iowa : John Deere Product Engineering Center, 2017.

35. **Loewenthal, Stuart H.** *Design of power transmitting shafts.* s.l. : NASA Reference Publication, 1984.

36. **W. Callister, David G., Rethwisch.** *Material science and Engineering.* s.l. : Wiley, 2011.

37. **Rafal Gradzki, Zbigniew Kulesza & Blazej Bartoszewicz.** *Method of shaft crack detection based on squared gain of vibration amplitude.* s.l. : Springer, 2019.

38. **Hariom1, Prof. Vijoy Kumar 2, Dr. Chandrababu D.** *A Review of Fundamental Shaft Failure Analysis.* s.l. : International Research Journal of Engineering and Technology, 2016. Vol. Volume: 03.

39. **Tabassian, R.** *Torsional vibration analysis of shafts based on A domaindecomposition method.* s.l. : Springer, 2013.

40. **R. Peretz, L. Rogel, J. Bortman, and R. Klein.** *Detection of Cracks in Shafts ia Analysis of Vibrations and Orbital Paths.* s.l. : Semantic Scholar, 2016.

41. **E. Downham, Ph and D., A.F.R.Ae.S.** *The Influence of Plain Bearings on Shaft Whirling Whirling.* s.l. : AERONAUTICAL RESEARCH COUNCIL REPORTS AND MEMORANDA, 1958. Vol. Technical Report No. 3046.

42. **Sanju Kumar, Rashmi Rao and B.A. Rajeevalochanam.** *CURRENT PRACTICES IN STRUCTURAL ANALYSIS AND TESTING OF AERO-ENGINE MAIN SHAFTS.* s.l. : Academic research paper on "Materials engineering", 2013.

43. **Desavale, R.G., Patil, A.M.** *Theoretical and Experimental Analysis of Torsional and Bending Effect on Four Cylinders Engine Crankshafts by Using Finite Element Approach.* s.l. : International Journal of Engineering Research, 2013.

44. **Ronald L. Eshleman, Ph.D., P.E.** *TORSIONAL VIBRATION OF MACHINE SYSTEMS.* s.l. : Clarendon Hills, Illinois, 1977.

45. **Freund, L. B.** *THE MECHANICS OF DYNAMIC FRACTURE*.* s.l. : Division of Engineering, Brown University, 1986. RI 02912.

46. **K.R Collins, R H and J Walter.** *Detection of shafts in rotating Timoshenko Shaft using Axial Impulses.* s.l. : ASME : Vibra Acoust Reliability, 1991.

47. **W.B. Wang, Z.S. Duan, X.L. Huang, B.C. Wen.** *The responses of the simple rotor with surface transverse crack.* New York : A. Muszynska, J.C. Simonis (Eds.), Rotating Machinery Dynamics, ASME, 1987. Vol. Vol. 2.

48. **D.E. Bently, A.S. Thomson.** *Detection of cracks in rotors.* Philadelphia : Incipient Failure Detection Conference, 1987.

49. **Nilsson, L.R.K.** *On the vibration behaviour of a cracked rotor.* Rome : Proceedings of the International Conference on Rotordynamic Problems in Power Plants, 1982.

50. **Sanderson, A.F.P.** *The vibration behaviour of a large steam turbine generator during crack propagation through the generator rotor.* London : Vibrations in Rotating Machinery, Institution of Mechanical Engineers Publications, 1992.

51. **I.W. Mayes, G.R. Davis.** *The vibrational behaviour of a rotating shaft system containing a transverse crack.* London : Vibrations in Rotating Machineries, Institution of Mechanical Engineers Publications, 1976.

52. **S. Hisa, H. Sakakida, H. Nakajima, K. Momoeda, T. Noda.** *Vibration diagnosis for large steam turbine rotor.* New York : Diagnostics Vehicle Dynamics and Special Topics,ASME, 1989.

53. **Nandi, A.** *Reduction of finite element equations for a rotor model on non isotropic spring support in a rotating frame.* s.l. : Finite Elem. Anal., 2004.

54. **E, Bouchbinder.** *Dynamic crack tip equation of motion.* s.l. : Phys Rev Lett, 2009.

55. **A, Mohammad.** *General harmonic balance solution of a cracked rotor-bearing-disk system for harmonic and subharmonic analysis: Analytical and Experimental approach.* s.l. : International Journal of Engineering Science, 2010. 48 921–935.

56. **Ke Xu, Xiongfei Wang, Haichao Cui and Fenggui Lu.** *nvestigation on LCF Behavior of Welded Joint at Diferent Temperatures for Bainite Steel.* s.l. : Chinese Journal of Mechanical Engineering, 2019.

57. **Dhamande, Vaibhav J SuryawanshiȦ* and L.S.** *Vibration Based Condition Assessment of Rotating cracked shaft using changes in critical speed and RMS Velocity response functions.* s.l. : international Journal of Current Engineering and Technology, 2014. ISSN 2277 – 4106.

58. **Amar, Mokhtar Adda-Bedia and Martine Ben.** *Crack dynamics in elastic media.* Paris Cedex 05, France : Laboratoire de Physique Statistique de l"Ecole Normale SupÂerieure, UnitÂe de Recherche associÂee au CNRS 1306,, 1999. F-75231.

59. **Anderson, T.L.** *Fracture Mechanics, 3rd Edition.* Boca Raton : CRC Press, 2017. ISBN 9781315370293.

60. **Darpe, Ashish K.** *Dynamics of a Jeffcott rotor with slant crack.* Delhi-110016, India, : Department of Mechanical Engineering, Indian Institute of Technology, 2007.

61. **Chen, Xuelian.** *Nonlinear responses analysis caused by slant crack in a rotor-bearing system.* s.l. : INTERNATIONAL LTD.JOURNAL OF VIBROENGINEERING, 2016. Vol. VOL. 18. ISSN 1392-8716.

62. **Roylance, David.** *Introduction to Fracture Mechanics.* Cambridge, MA 02139 : Department of Materials Science and Engineering, 2001.

63. **ABAQUS.** 2006.

64. **Speed, Whirling of Shafts and Critical.** s.l. : Theory of MachinesMotion. TM1001.

65. **www.google.com, Whirling machine.** [Online]

66. **LMX05, SPECTROMAXx.** *Metal Analysis without.* s.l. : AMETEK, Material Analysis Division.

67. **Wiele, Brandon.** *Carbon Steel Grades.*

68. **Lissenden, C. J., Tissot, S. P., Trethewey, M. W., and Maynard, K. P.** *Torsion response of a cracked stainless steel shaft.* s.l. : Engineering Science and MechanicsMaterials Research Institute (MRI)Mechanical Engineering, 2007.

69. **Roylance, David.** *Introduction to Fracture Mechanics.* s.l. : Department of Materials Science and Engineering Massachusetts Institute of Technology Cambridge, 2001. MA 02139.

70. **Hellan, K.** *Introduction to Fracture Mechanics.* s.l. : McGraw-Hill Book Co., 1985.

APPENDIX I

Specimen I

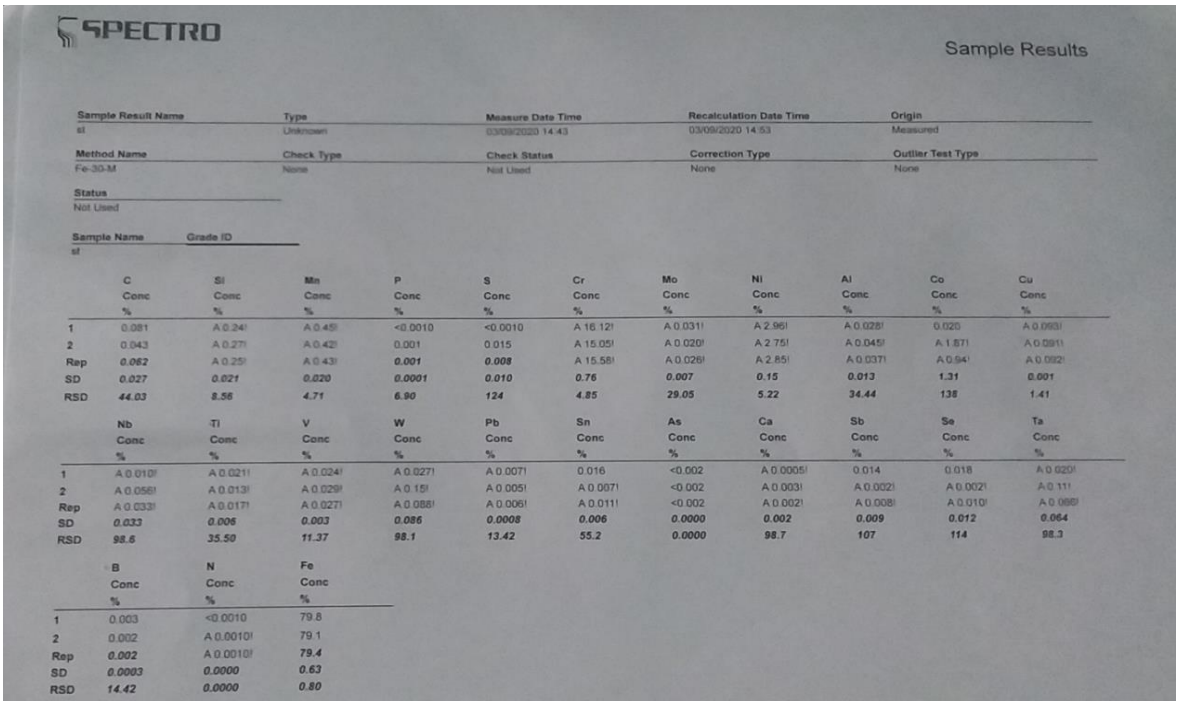

SPECTRO

Sample Results

Sample Result Name	Type	Measure Date Time	Recalculation Date Time	Origin
sl	Unknown	03/09/2020 14:43	03/09/2020 14:53	Measured

Method Name	Check Type	Check Status	Correction Type	Outlier Test Type
Fe-30-M	None	Not Used	None	None

Status: Not Used

Sample Name: sl — Grade ID:

	C Conc %	Si Conc %	Mn Conc %	P Conc %	S Conc %	Cr Conc %	Mo Conc %	Ni Conc %	Al Conc %	Co Conc %	Cu Conc %
1	0.081	A 0.24|	A 0.45|	<0.0010	<0.0010	A 16.12|	A 0.031|	A 2.96|	A 0.028|	0.020	A 0.093|
2	0.043	A 0.27|	A 0.42|	0.001	0.015	A 15.05|	A 0.020|	A 2.75|	A 0.045|	A 1.87|	A 0.091|
Rep	*0.062*	A 0.25|	A 0.43|	*0.001*	*0.008*	A 15.58|	A 0.026|	A 2.85|	A 0.037|	A 0.94|	A 0.092|
SD	*0.027*	*0.021*	*0.020*	*0.0001*	*0.010*	*0.76*	*0.007*	*0.15*	*0.013*	*1.31*	*0.001*	
RSD	*44.03*	*8.56*	*4.71*	*6.90*	*124*	*4.85*	*29.05*	*5.22*	*34.44*	*138*	*1.41*	

	Nb Conc %	Ti Conc %	V Conc %	W Conc %	Pb Conc %	Sn Conc %	As Conc %	Ca Conc %	Sb Conc %	Se Conc %	Ta Conc %
1	A 0.010|	A 0.021|	A 0.024|	A 0.027|	A 0.007|	0.016	<0.002	A 0.0005|	0.014	0.018	A 0.020|
2	A 0.056|	A 0.013|	A 0.029|	A 0.15|	A 0.005|	A 0.007|	<0.002	A 0.003|	A 0.002|	A 0.002|	A 0.11|
Rep	A 0.033|	A 0.017|	A 0.027|	A 0.088|	A 0.006|	A 0.011|	<0.002	A 0.002|	A 0.008|	A 0.010|	A 0.065|
SD	*0.033*	*0.006*	*0.003*	*0.086*	*0.0008*	*0.006*	*0.0000*	*0.002*	*0.009*	*0.012*	*0.064*	
RSD	*98.6*	*35.50*	*11.37*	*98.1*	*13.42*	*55.2*	*0.0000*	*98.7*	*107*	*114*	*98.3*	

	B Conc %	N Conc %	Fe Conc %
1	0.003	<0.0010	79.8
2	0.002	A 0.0010|	79.1
Rep	*0.002*	A 0.0010|	*79.4*
SD	*0.0003*	*0.0000*	*0.63*
RSD	*14.42*	*0.0000*	*0.80*

Specimen II

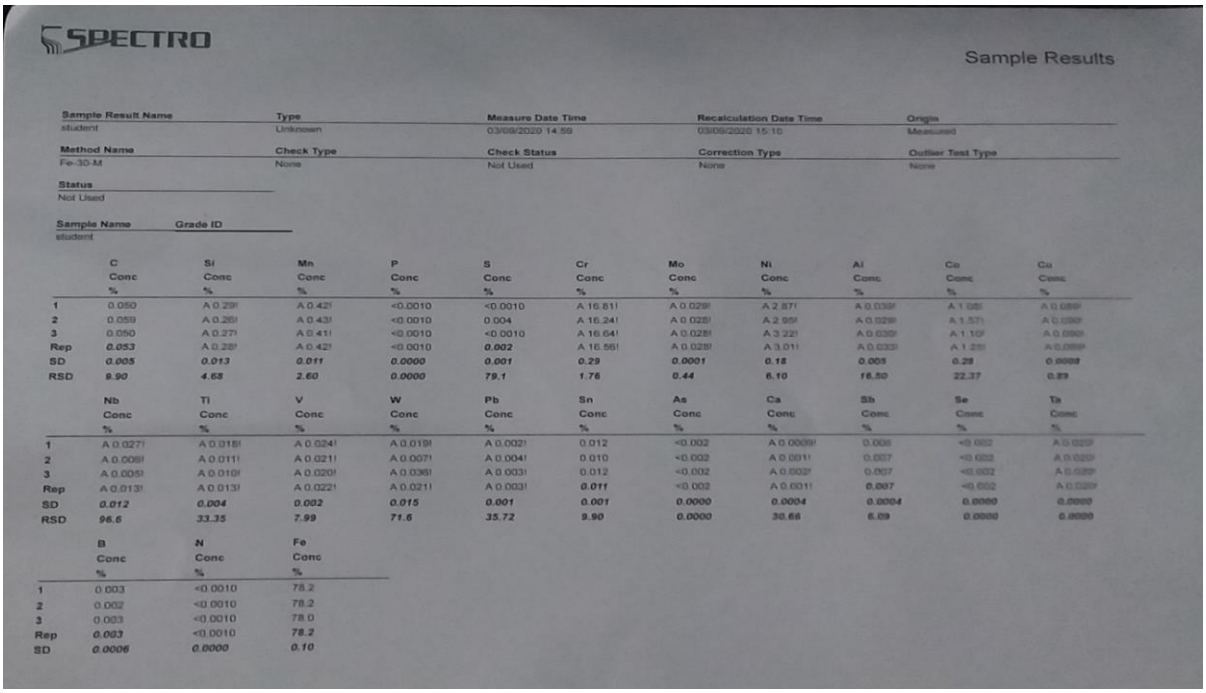

SPECTRO

Sample Results

Sample Result Name	Type	Measure Date Time	Recalculation Date Time	Origin
student	Unknown	03/09/2020 14:59	03/09/2020 15:10	Measured

Method Name	Check Type	Check Status	Correction Type	Outlier Test Type
Fe-30-M	None	Not Used	None	None

Status: Not Used

Sample Name: student — Grade ID:

	C Conc %	Si Conc %	Mn Conc %	P Conc %	S Conc %	Cr Conc %	Mo Conc %	Ni Conc %	Al Conc %	Co Conc %	Cu Conc %
1	0.050	A 0.29|	A 0.42|	<0.0010	<0.0010	A 16.81|	A 0.029|	A 2.87|	A 0.030|	A 1.58|	A 0.089|
2	0.059	A 0.26|	A 0.43|	<0.0010	0.004	A 16.24|	A 0.028|	A 2.95|	A 0.029|	A 1.57|	A 0.090|
3	0.050	A 0.27|	A 0.41|	<0.0010	<0.0010	A 16.64|	A 0.028|	A 3.22|	A 0.030|	A 1.10|	A 0.090|
Rep	*0.053*	A 0.28|	A 0.42|	<0.0010	*0.002*	A 16.56|	A 0.028|	A 3.01|	A 0.033|	A 1.25|	A 0.089|
SD	*0.005*	*0.013*	*0.011*	*0.0000*	*0.001*	*0.29*	*0.0001*	*0.18*	*0.005*	*0.28*	*0.0009*	
RSD	*9.90*	*4.68*	*2.60*	*0.0000*	*79.1*	*1.76*	*0.44*	*6.10*	*16.50*	*22.37*	*0.89*	

	Nb Conc %	Ti Conc %	V Conc %	W Conc %	Pb Conc %	Sn Conc %	As Conc %	Ca Conc %	Sb Conc %	Se Conc %	Ta Conc %
1	A 0.027|	A 0.018|	A 0.024|	A 0.019|	A 0.002|	0.012	<0.002	A 0.0009|	0.006	<0.002	A 0.020|
2	A 0.008|	A 0.011|	A 0.021|	A 0.007|	A 0.004|	0.010	<0.002	A 0.001|	0.007	<0.002	A 0.020|
3	A 0.005|	A 0.010|	A 0.020|	A 0.036|	A 0.003|	0.012	<0.002	A 0.002|	0.007	<0.002	A 0.020|
Rep	A 0.013|	A 0.013|	A 0.022|	A 0.021|	A 0.003|	*0.011*	<0.002	A 0.001|	*0.007*	<0.002	A 0.020|
SD	*0.012*	*0.004*	*0.002*	*0.015*	*0.001*	*0.001*	*0.0000*	*0.0004*	*0.0004*	*0.0000*	*0.0000*	
RSD	*96.6*	*33.35*	*7.99*	*71.6*	*35.72*	*9.90*	*0.0000*	*30.66*	*6.09*	*0.0000*	*0.0000*	

	B Conc %	N Conc %	Fe Conc %
1	0.003	<0.0010	78.2
2	0.002	<0.0010	78.2
3	0.003	<0.0010	78.0
Rep	*0.003*	<0.0010	*78.2*
SD	*0.0006*	*0.0000*	*0.10*

APPENDIX II

For the following 151 elemental sets, displacements in x, y and z directions are depicted in the following graphs below.

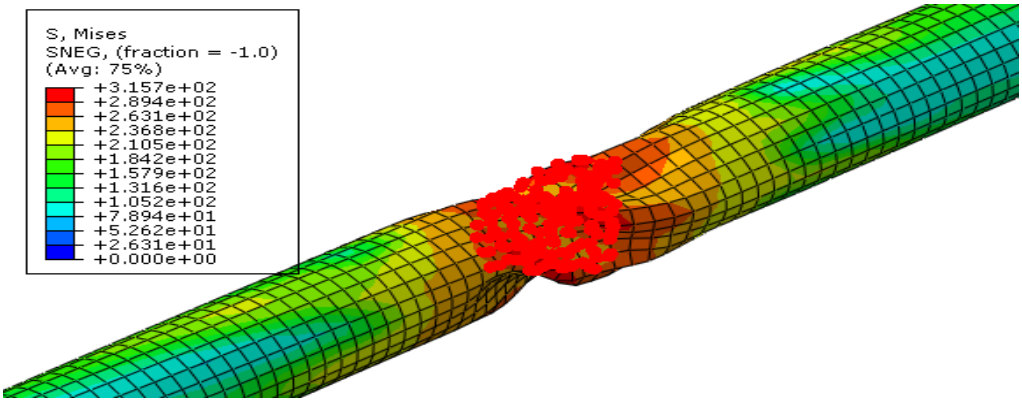

Figure a : Element Nodal

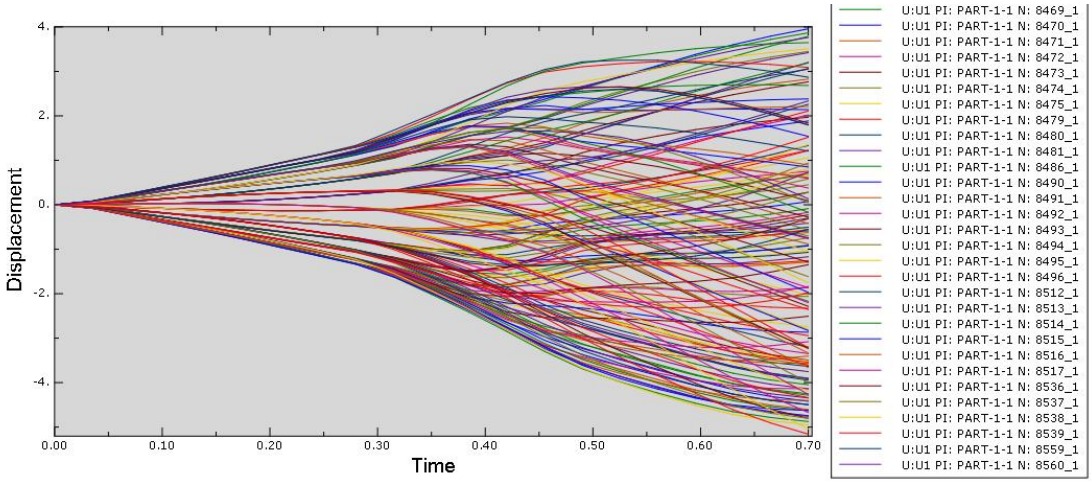

Figure b: displacement versus time graph in x_ direction in mm

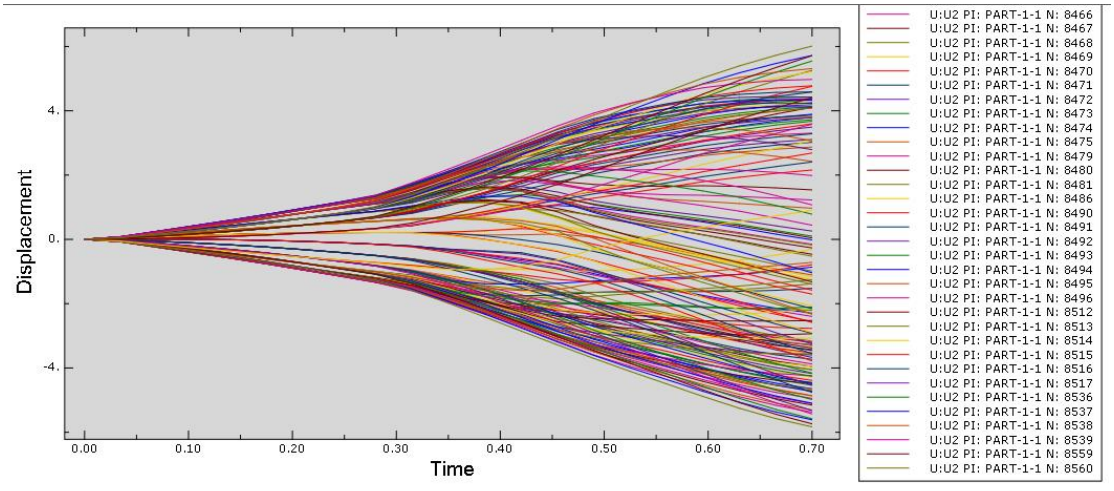

Figure c: displacement versus time graph in y_ direction in mm

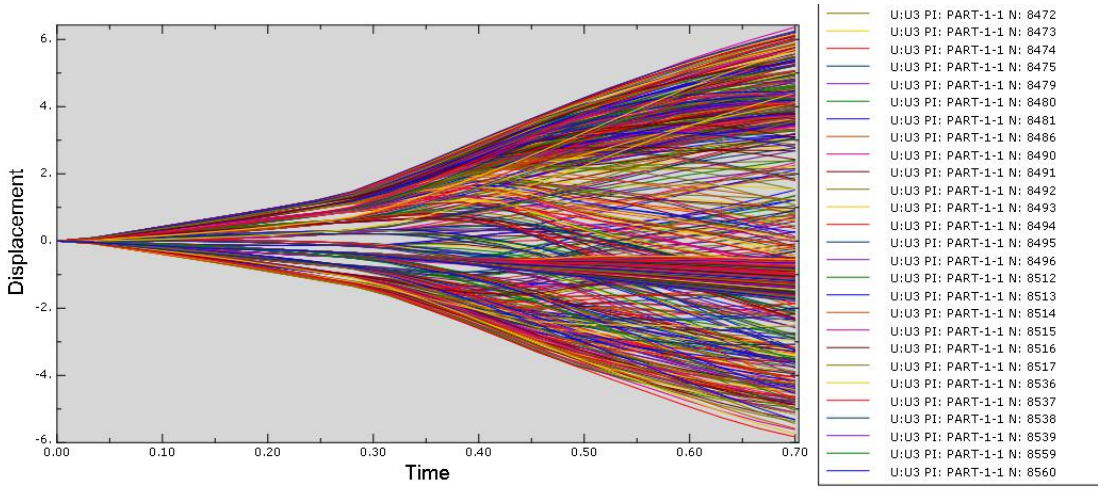

Figure d: displacement versus time graph in z_ direction in mm

APPENDIX III

U:U2 PI: PART-1-1 N: nodes

From Field Data: U:U2 at part instance PART-1-1 for different nodes

X_Steps	N-6909	N-5325	N-5383	N-5430	N-5466	N-5994	N-5453
0	0	0	0	0	0	0	0
0.035064	0.00019	-0.04766	0.042769	0.025173	0.007355	0.084197	0.025692
0.070073	0.124676	-0.15641	0.132738	0.072983	0.02841	0.253097	0.073424
0.105062	0.274128	-0.26021	0.217085	0.114149	0.056737	0.423639	0.114537
0.14005	0.421177	-0.35873	0.295458	0.148345	0.092494	0.595348	0.148676
0.175039	0.576598	-0.45619	0.371041	0.176735	0.137549	0.775397	0.17697
0.210028	0.727297	-0.5512	0.442627	0.197825	0.194025	0.965854	0.197999
0.245016	0.865186	-0.63784	0.505486	0.20977	0.259436	1.15663	0.20985
0.280005	0.999373	-0.71734	0.560933	0.213098	0.335641	1.36188	0.213392
0.315167	1.12887	-0.79105	0.620726	0.212797	0.457172	1.70373	0.206432
0.350153	1.25267	-0.87367	0.700526	0.146757	0.611854	2.07894	0.124561
0.385106	1.37131	-0.9176	0.717727	-0.00036	0.762695	2.45627	-0.01467
0.420097	1.48109	-0.92777	0.604434	-0.17403	0.966373	2.86865	-0.16728
0.455053	1.55973	-0.96868	0.441006	-0.3772	1.27514	3.29536	-0.34727
0.490129	1.64301	-1.01725	0.242344	-0.66024	1.62226	3.62717	-0.67524
0.525017	1.72298	-1.00899	0.016134	-0.96142	1.95859	3.8624	-1.05646
0.560154	1.81594	-0.9721	-0.20256	-1.26395	2.30791	4.062	-1.4259
0.595075	1.91422	-0.91059	-0.44037	-1.59861	2.66718	4.22573	-1.80568
0.630168	2.00193	-0.83757	-0.68887	-1.94007	2.98715	4.3083	-2.18505
0.665089	2.07034	-0.74421	-0.9401	-2.27647	3.29145	4.34248	-2.55751
0.7	2.11591	-0.6425	-1.16452	-2.58371	3.5815	4.32561	-2.89873

APPENDIX IV

U:U1 PI: PART-1-1 N: nodes

From Field Data: U:U1 at part instance PART-1-1 for different nodes

X_Time	N-8136	N-8137	N-8138	N-8159	N-8160	N-8161	N-8162	N-8181	N-8182	N-8183	N-8205	N-8206	N-8207	N-8208	N-8560	N-8561	N-8582
0	0	0	0	0	0	0	0	0	0	0	0	0	0	0	0	0	0
0.035064	-0.02941	-0.01486	0.000795	-0.03022	-0.01525	0.000851	0.016889	-0.04412	-0.03103	-0.01564	-0.03184	-0.01603	0.000976	0.017905	0.072297	0.055232	0.085575
0.070073	-0.10976	-0.05216	0.009311	-0.11054	-0.0525	0.009426	0.070654	-0.16153	-0.11132	-0.05285	-0.11209	-0.05319	0.009659	0.071792	0.204909	0.154401	0.241816
0.105062	-0.18435	-0.08276	0.024962	-0.18507	-0.08303	0.025165	0.131495	-0.2745	-0.18579	-0.0833	-0.18651	-0.08357	0.025572	0.132817	0.333895	0.248387	0.396247
0.14005	-0.25274	-0.10633	0.047963	-0.25342	-0.10654	0.048238	0.199438	-0.38259	-0.25409	-0.10675	-0.25477	-0.10695	0.0488	0.200925	0.458756	0.336741	0.54837
0.175039	-0.31794	-0.12366	0.079799	-0.31854	-0.12379	0.080135	0.27811	-0.49067	-0.31914	-0.12392	-0.31973	-0.12405	0.080833	0.27971	0.584306	0.422736	0.704149
0.210028	-0.37776	-0.1326	0.12239	-0.37829	-0.13265	0.122826	0.369182	-0.59686	-0.37884	-0.13271	-0.37938	-0.13276	0.123709	0.370988	0.711209	0.506157	0.865174
0.245016	-0.42851	-0.13276	0.172821	-0.42903	-0.13272	0.173422	0.466689	-0.69455	-0.42954	-0.13267	-0.43006	-0.13262	0.17465	0.468947	0.833571	0.582807	1.02577
0.280005	-0.47126	-0.12403	0.232363	-0.47178	-0.12389	0.233159	0.572849	-0.78576	-0.47229	-0.12374	-0.4728	-0.1236	0.234763	0.575639	0.993284	0.682394	1.25754
0.315167	-0.50509	-0.10594	0.300927	-0.50561	-0.10566	0.301977	0.687096	-0.86952	-0.50613	-0.10531	-0.5067	-0.10494	0.304347	0.690812	1.20674	0.80521	1.55481
0.350153	-0.52987	-0.07879	0.378068	-0.53045	-0.07834	0.379339	0.809325	-0.9463	-0.53065	-0.07704	-0.53124	-0.07473	0.385601	0.817088	1.38655	0.90061	1.82143
0.385106	-0.55266	-0.04872	0.467096	-0.54588	-0.046	0.463125	0.949844	-1.01327	-0.53693	-0.02988	-0.53171	-0.01177	0.496951	0.962623	1.5521	0.947406	2.07781
0.420097	-0.55772	0.002943	0.567913	-0.55499	0.004169	0.565853	1.09037	-1.07958	-0.55168	0.018171	-0.55187	0.033866	0.603243	1.11046	1.65095	0.89787	2.3049
0.455053	-0.54591	0.066703	0.680079	-0.54598	0.069144	0.683397	1.2415	-1.11092	-0.54649	0.083636	-0.55135	0.09889	0.733919	1.27719	1.66046	0.767685	2.44513
0.490129	-0.48236	0.18325	0.835189	-0.48481	0.189282	0.846272	1.42152	-1.10729	-0.4876	0.207521	-0.49751	0.228338	0.920187	1.47814	1.61367	0.547415	2.52497
0.525017	-0.41609	0.308431	1.00326	-0.41937	0.316322	1.01841	1.61486	-1.1151	-0.42213	0.33787	-0.43713	0.35864	1.10188	1.68099	1.52216	0.281694	2.54465
0.560154	-0.37286	0.41037	1.15328	-0.37716	0.418487	1.16908	1.79824	-1.14308	-0.38145	0.440103	-0.40207	0.458634	1.25379	1.86641	1.34138	-0.04753	2.48431
0.595075	-0.3466	0.496217	1.29114	-0.35221	0.503485	1.30715	1.97786	-1.18699	-0.35874	0.523932	-0.38445	0.539408	1.39085	2.0468	1.08797	-0.41875	2.3448
0.630168	-0.3266	0.57198	1.40992	-0.33279	0.578947	1.42638	2.12612	-1.23709	-0.3425	0.597884	-0.37492	0.610704	1.51095	2.19876	0.804782	-0.81044	2.17776
0.665089	-0.3143	0.626328	1.50043	-0.32158	0.632589	1.51708	2.24252	-1.27898	-0.33499	0.650057	-0.37489	0.662162	1.60206	2.31669	0.489864	-1.21066	1.97202
0.7	-0.30269	0.667991	1.56689	-0.31051	0.674619	1.58516	2.32594	-1.30556	-0.32747	0.69134	-0.37339	0.704257	1.67551	2.40684	0.136159	-1.63382	1.72631

APPENDIX V

U:U2 PI: PART-1-1 N: nodes

From Field Data: U:U2 at part instance PART-1-1 for different nodes

X_Time	N-8136	N-8137	N-8138	N-8159	N-8160	N-8161	N-8162	N-8181	N-8182	N-8183	N-8205	N-8206	N-8207	N-8208	N-8560	N-8561	N-8582
0	0	0	0	0	0	0	0	0	0	0	0	0	0	0	0	0	0
0.035064	-0.04989	-0.05597	-0.05791	-0.05133	-0.05758	-0.05956	-0.05712	-0.04245	-0.05278	-0.0592	-0.05423	-0.06081	-0.06288	-0.06029	0.053316	0.070844	0.032449
0.070073	-0.1984	-0.22065	-0.22654	-0.1999	-0.22231	-0.22823	-0.21723	-0.16391	-0.20141	-0.22398	-0.20292	-0.22564	-0.23162	-0.22042	0.159044	0.208429	0.098566
0.105062	-0.35117	-0.38789	-0.39583	-0.35275	-0.3896	-0.39755	-0.37602	-0.29106	-0.35432	-0.39131	-0.3559	-0.39303	-0.401	-0.37923	0.271031	0.35106	0.171706
0.14005	-0.50787	-0.55722	-0.56525	-0.50951	-0.55899	-0.567	-0.53296	-0.42364	-0.51115	-0.56075	-0.5128	-0.56251	-0.57051	-0.53619	0.389173	0.498502	0.251885
0.175039	-0.67628	-0.73699	-0.74302	-0.67791	-0.73871	-0.74472	-0.69548	-0.56824	-0.67955	-0.74045	-0.68121	-0.74221	-0.74816	-0.69861	0.518517	0.65691	0.342635
0.210028	-0.85656	-0.92671	-0.92813	-0.85828	-0.92851	-0.92987	-0.86226	-0.72589	-0.86001	-0.93033	-0.86175	-0.93215	-0.93341	-0.86542	0.662204	0.829486	0.446947
0.245016	-1.03699	-1.11416	-1.10868	-1.03901	-1.11624	-1.11067	-1.02272	-0.8865	-1.04103	-1.11832	-1.04305	-1.12041	-1.11466	-1.02623	0.81471	1.00934	0.56163
0.280005	-1.22148	-1.30334	-1.2885	-1.22382	-1.30573	-1.29076	-1.18005	-1.05322	-1.22616	-1.30811	-1.22847	-1.31047	-1.29523	-1.18389	1.0208	1.25042	0.735365
0.315167	-1.40874	-1.49286	-1.46622	-1.41149	-1.49564	-1.46882	-1.3331	-1.22511	-1.41434	-1.49852	-1.41723	-1.50142	-1.47418	-1.33771	1.38719	1.65727	1.04383
0.350153	-1.59939	-1.68344	-1.64271	-1.60418	-1.68824	-1.64737	-1.48433	-1.40623	-1.61	-1.6942	-1.6177	-1.70202	-1.66079	-1.49743	1.7967	2.09502	1.39761
0.385106	-1.81115	-1.89371	-1.83375	-1.82437	-1.90716	-1.85077	-1.64975	-1.62054	-1.83784	-1.9201	-1.85151	-1.93216	-1.87556	-1.69113	2.23587	2.56117	1.78924
0.420097	-1.96286	-2.03952	-1.95971	-1.97421	-2.05101	-1.97368	-1.7431	-1.76008	-1.98592	-2.06125	-1.99771	-2.07052	-1.98957	-1.77411	2.69951	3.03933	2.20616
0.455053	-2.08117	-2.14964	-2.04756	-2.09167	-2.15994	-2.05818	-1.79908	-1.87268	-2.10297	-2.16782	-2.11419	-2.17569	-2.06285	-1.81813	3.1831	3.51738	2.66243
0.490129	-2.17687	-2.23452	-2.11247	-2.18624	-2.24205	-2.11813	-1.84345	-1.9619	-2.19604	-2.24634	-2.20734	-2.24942	-2.10453	-1.84697	3.67221	3.97794	3.149
0.525017	-2.28109	-2.32342	-2.17679	-2.28922	-2.32839	-2.17854	-1.88351	-2.06247	-2.29764	-2.32887	-2.30963	-2.32897	-2.15232	-1.87553	4.14438	4.38771	3.63488
0.560154	-2.42807	-2.45163	-2.27426	-2.43588	-2.45487	-2.27366	-1.94524	-2.21225	-2.44388	-2.45302	-2.45786	-2.45124	-2.23866	-1.92929	4.59601	4.75517	4.11288
0.595075	-2.61431	-2.61496	-2.40014	-2.62222	-2.61698	-2.39705	-2.02174	-2.40638	-2.63041	-2.61335	-2.64713	-2.61036	-2.35293	-1.99689	5.02168	5.0893	4.5715
0.630168	-2.77235	-2.74786	-2.49828	-2.78069	-2.74883	-2.49306	-2.08135	-2.57791	-2.79019	-2.74439	-2.81186	-2.74074	-2.43936	-2.04466	5.39735	5.35067	5.00151
0.665089	-2.88814	-2.84202	-2.56025	-2.89766	-2.84307	-2.55379	-2.10697	-2.70917	-2.91004	-2.83883	-2.93818	-2.83409	-2.493	-2.06275	5.72432	5.55845	5.39784
0.7	-2.96773	-2.90471	-2.59903	-2.97731	-2.90454	-2.58967	-2.1202	-2.80001	-2.9918	-2.89951	-3.02504	-2.89199	-2.51671	-2.0622	6.01168	5.71422	5.77373

APPENDIX VI

U:U3 PI: PART-1-1 N: nodes

From Field Data: U:U3 at part instance PART-1-1 for different nodes

X_Time	N-8136	N-8137	N-8138	N-8159	N-8160	N-8161	N-8162	N-8181	N-8182	N-8183	N-8205	N-8206	N-8207	N-8208	N-8560	N-8561	N-8582
0	0	0	0	0	0	0	0	0	0	0	0	0	0	0	0	0	0
0.035064	-0.03538	-0.03538	-0.03538	-0.03574	-0.03574	-0.03574	-0.03574	-0.03609	-0.03609	-0.03609	-0.03645	-0.03645	-0.03645	-0.03645	-0.04206	-0.04206	-0.04242
0.070073	-0.09305	-0.09305	-0.09305	-0.0934	-0.0934	-0.0934	-0.0934	-0.09375	-0.09375	-0.09375	-0.0941	-0.0941	-0.0941	-0.0941	-0.09985	-0.09985	-0.10021
0.105062	-0.15089	-0.15089	-0.15089	-0.15125	-0.15125	-0.15125	-0.15125	-0.15161	-0.15161	-0.15161	-0.15197	-0.15197	-0.15197	-0.15197	-0.15781	-0.15781	-0.15818
0.14005	-0.20885	-0.20885	-0.20885	-0.20922	-0.20922	-0.20922	-0.20922	-0.20959	-0.20959	-0.20959	-0.20996	-0.20996	-0.20996	-0.20996	-0.21594	-0.21595	-0.21632
0.175039	-0.23541	-0.23541	-0.23541	-0.23606	-0.23606	-0.23605	-0.23605	-0.23671	-0.23671	-0.2367	-0.23735	-0.23735	-0.23735	-0.23734	-0.2473	-0.24731	-0.24794
0.210028	-0.24786	-0.24786	-0.24785	-0.24839	-0.24839	-0.24838	-0.24837	-0.24893	-0.24892	-0.24892	-0.24947	-0.24946	-0.24946	-0.24945	-0.25926	-0.25926	-0.25996
0.245016	-0.29777	-0.29776	-0.29774	-0.29833	-0.29833	-0.29831	-0.29829	-0.2989	-0.2989	-0.29889	-0.29946	-0.29946	-0.29944	-0.29943	-0.30949	-0.30952	-0.31047
0.280005	-0.34366	-0.34362	-0.34357	-0.34432	-0.34428	-0.34423	-0.34419	-0.345	-0.34498	-0.34494	-0.34563	-0.34559	-0.34554	-0.34549	-0.37236	-0.37248	-0.3799
0.315167	-0.38978	-0.38967	-0.38958	-0.39052	-0.39042	-0.39032	-0.39025	-0.39133	-0.39128	-0.39119	-0.39205	-0.39198	-0.39186	-0.3918	-0.47339	-0.47351	-0.48139
0.350153	-0.43652	-0.43665	-0.43662	-0.43767	-0.43782	-0.43784	-0.43766	-0.43898	-0.43902	-0.43927	-0.44074	-0.44115	-0.44148	-0.44149	-0.57861	-0.57664	-0.58688
0.385106	-0.48139	-0.48009	-0.47808	-0.48461	-0.48404	-0.48175	-0.47951	-0.48658	-0.4876	-0.48818	-0.49057	-0.49177	-0.49221	-0.49009	-0.68439	-0.68189	-0.69337
0.420097	-0.50708	-0.50409	-0.50002	-0.51039	-0.50807	-0.50345	-0.49964	-0.51271	-0.51346	-0.51214	-0.51658	-0.51567	-0.51342	-0.50938	-0.80034	-0.7983	-0.80768
0.455053	-0.49921	-0.49532	-0.49056	-0.5025	-0.49915	-0.49358	-0.49034	-0.50453	-0.50544	-0.50318	-0.50845	-0.50681	-0.50318	-0.49891	-0.91977	-0.91705	-0.92545
0.490129	-0.47619	-0.471	-0.46591	-0.47969	-0.47484	-0.46869	-0.46646	-0.48251	-0.48278	-0.4791	-0.48632	-0.48286	-0.47836	-0.47365	-1.03708	-1.03414	-1.03872
0.525017	-0.47046	-0.46376	-0.45774	-0.47404	-0.46772	-0.46054	-0.4577	-0.47802	-0.47724	-0.47217	-0.48151	-0.47591	-0.47078	-0.46446	-1.14968	-1.13949	-1.14557
0.560154	-0.48838	-0.4807	-0.47372	-0.49198	-0.48474	-0.47646	-0.47265	-0.49634	-0.49537	-0.48918	-0.50018	-0.49307	-0.48697	-0.47925	-1.26352	-1.24376	-1.25256
0.595075	-0.50801	-0.49938	-0.49128	-0.51167	-0.50344	-0.49397	-0.48905	-0.51627	-0.51524	-0.50784	-0.52046	-0.5119	-0.50449	-0.4956	-1.37489	-1.34735	-1.36036
0.630168	-0.53038	-0.5212	-0.51243	-0.53403	-0.52533	-0.51504	-0.50917	-0.53817	-0.53772	-0.52977	-0.54376	-0.53401	-0.52585	-0.51535	-1.49336	-1.45286	-1.47195
0.665089	-0.55503	-0.54588	-0.53697	-0.5586	-0.55004	-0.53947	-0.5332	-0.56113	-0.56257	-0.55439	-0.56912	-0.55838	-0.55076	-0.53927	-1.60925	-1.55607	-1.58131
0.7	-0.57201	-0.56239	-0.55309	-0.57563	-0.56652	-0.55546	-0.54886	-0.57761	-0.57979	-0.57085	-0.58674	-0.5745	-0.56769	-0.55477	-1.72234	-1.65549	-1.68892

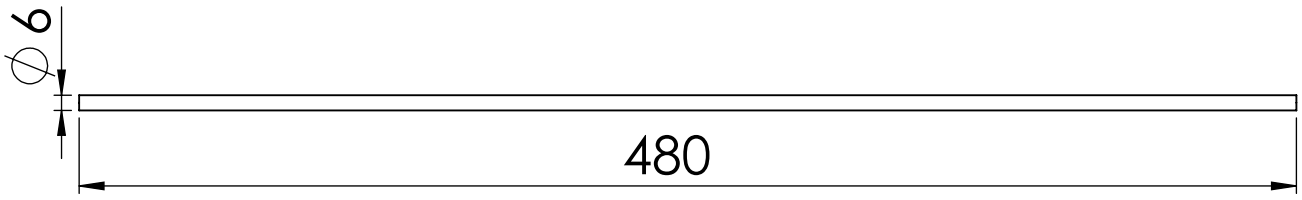

SHAFT

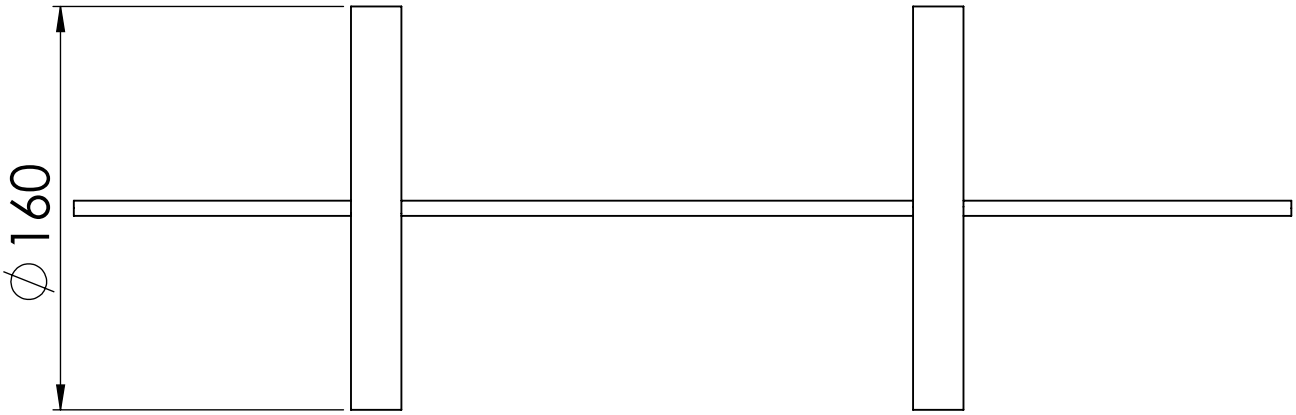

SHAFT-MASS ASSEMBLY

DR.BY. SEMIHAR AYALEW		ADDIS ABABA INSTITUTE OF	DR.NO.
CHKD.BY.		TECHNOLOGY	1
DATE	SCALE	TITLE	
Sep, 2020	1:2	FRONT VIEW	